

Fission barriers and probabilities of spontaneous fission for elements with $Z \geq 100$

A. Baran¹, M. Kowal^b, P.-G. Reinhard^d, L.M. Robledo^c, A. Staszczak¹, M. Warda¹

^aUniversity of Maria-Curie-Skłodowska, 20031 Lublin, Poland

^bNational Centre for Nuclear Research, Hoża 69, PL-00-681 Warsaw, Poland

^cDepartamento de Física Teórica, Universidad Autónoma de Madrid, 28049 Madrid, Spain

^dInstitute of Theoretical Physics, University of Erlangen-Nuremberg, Germany

Abstract

This is a short review of methods and results of calculations of fission barriers and fission half-lives of even-even superheavy nuclei. An approvable agreement of the following approaches is shown and discussed: The macroscopic-microscopic approach based on the stratagem of the shell correction to the liquid drop model and a vantage point of microscopic energy density functionals of Skyrme and Gogny type selfconsistently calculated within Hartree-Fock-Bogoliubov method. Mass parameters are calculated in the Hartree-Fock-Bogoliubov cranking approximation. A short part of the paper is devoted to the nuclear fission dynamics. We also discuss the predictive power of Skyrme functionals applied to key properties of the fission path of ^{266}Hs . It applies the standard techniques of error estimates in the framework of a χ^2 analysis.

Keywords: Fission barriers; fission half-lives; selfconsistent methods; macroscopic-microscopic method; Skyrme functional; Gogny functional

1. Introduction

Considerable progress in the experimental synthesis of heaviest nuclei has been achieved recently by the Flerov Laboratory in Dubna [1, 2, 3, 4, 5, 6, 7, 8, 9, 10, 11] and was partially confirmed in the laboratories at GSI [12, 13, 14, 15, 16], LBNL [17] and RIKEN [18]. Nonetheless, the fundamental question of what is the largest possible atomic number of an atomic nucleus is still unanswered. For example, at the time of writing this manuscript the heaviest identified super-heavy element is $Z = 118$, but even larger elements are not yet excluded. Due to substantial Coulomb repulsion for super-heavy nuclei the stability decreases rapidly when going up in system size. Only shell effects allow super-heavy (SH) nuclei with $Z \geq 100$ to survive. There are two dominant processes of disintegration for such heavy systems: alpha particle emission and fission. It is the subject of this contribution to provide an overview of the state of the art relating to the latter process, fission of SH nuclei. Two different microscopic methods for estimating the stability of SH nuclei are used. There are, on the one hand, the self-consistent approaches using effective interactions as, e.g., the Hartree-Fock (HF) plus BCS (HFBCS) or Hartree-Fock-Bogoliubov (HFB) method, and, on the other hand the more phenomenological macroscopic-microscopic (MM) method. The latter is less demanding and thus allows even extensive studies of multidimensional fission landscapes. Although these models differ quantitatively, they agree in predicted topological properties as, e.g., the prolate deformed SH nuclei with $Z = 100 - 112$

and $N \leq 170$, which are confirmed experimentally for nuclei around ^{254}No [19] and spherical or oblate deformed systems with $N = 174 - 184$ (see [20, 21]).

The height of the fission barrier, B_f , is one of the most important ingredients to calculate the survival probability of SH elements synthesised in heavy-ion reactions. It allows to estimate the competition between the fission process and particle emission. To evaluate B_f , one needs the energy as function of collective deformation, the potential energy surfaces (PES). Ideally, one has to figure out all competing minima and saddle points on multidimensional maps. Having preconceived ideas about the expected fission landscape, one usually one restricts the search to a one-dimensional fission path. In any case, the PES is the basic ingredient for the evaluation of fission half-life (HL).

The last review of theoretical properties of SH elements covering MM and self-consistent models was published eight years ago [22]. Since then substantial progress has been made in the development of models and methods especially by Lublin-Madrid collaboration [23, 24], Lublin-Oak Ridge-Warsaw group [25, 26, 27, 28, 29, 30], and Erlangen-Darmstadt team [31] – energy density functional (EDF) HFB approaches – and in the MM model by the Warsaw [32, 33, 34], Los Alamos school [35] and the relativistic mean-field (RMF) [36].

In this paper, we are discussing methods to obtain the PES, barrier heights, mass parameters and fission HLs using modern approaches like the shell correction method in a multidimensional space of deformations and/or the method of energy density functionals (EDF) of Skyrme and Gogny types treated self-consistently in the HFB framework. The main purpose is a comparison of results of these different approaches and the discussion of uncertainties that affect the data in the process of calculation.

The paper is outlined as follows: Section 2.1 deals with MM methods and data. In Section 2.2, we deliver the discussion of microscopic Skyrme’s and Gogny’s functionals approaches and results. The short Section 2.3 tackles the issue of mass parameters and their effect on the HLs. Section 3 relates the calculated data to the experimentally known cases. Section 3.2 deals with an influence of dynamical treatment of fission process based on the action minimisation on fission half-lives. Section 4 discusses an estimate of extrapolation errors for the various observables. Conclusions are given in Section 5.

2. Predictions for barriers and life-times

2.1. Macroscopic-microscopic (MM) approach

The MM model composes the total energy of the nucleus from two complementary parts. One is the macroscopic energy, usually some version of a liquid drop (LD) energy and the other the shell correction which describes the influence of single particles (SP) energies and their quantum shell structure beyond the LD. Both parts are modelled independently. The LD part is taken from the extensive fits within the LD model. The results discussed here were obtained within a MM model based on the single particle (SP) spectrum of a deformed Woods-Saxon potential [37]. The SP spectrum obtained from the deformed Woods-Saxon potential is used as input to compute the Strutinsky shell correction energy [38, 39]. For the macroscopic part we used the Yukawa plus exponential model [40]. The pairing parameters and three parameters of the macroscopic energy formula were determined in [41] by a fit to masses of even-even nuclei with $Z \geq 84$ and $N > 126$ as given in [42].

In Figure 1 we display the height of the first fission barriers B_f for these nuclei calculated within the MM model as the difference between the lowest saddle point energy and the ground

state one E_I . It can be seen that in the whole region of considered nuclei the barriers are smaller than 7 MeV. The highest values are obtained for the nuclei $^{270}108_{162}$, $^{292}114_{178}$ and around the nucleus $Z \approx 100, N \approx 150$.

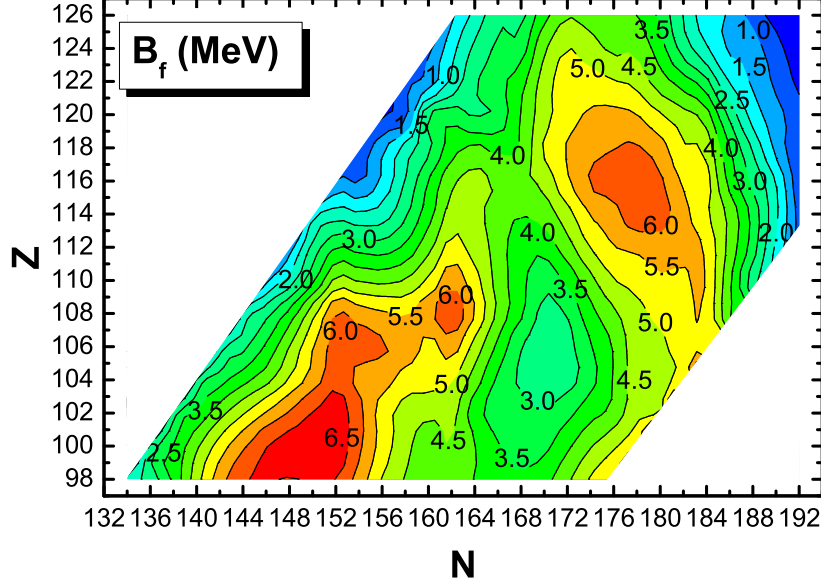


Figure 1: Contour map of calculated fission barrier heights B_f for even-even superheavy nuclei.

Another important observation concerns the behaviour of fission barrier heights with increasing proton number of these heaviest nuclei. One can recognise that the quite high barrier for $^{296}118_{178}$ rapidly decreases reaching a value 1.43 MeV for the $^{312}126_{186}$ nucleus. Obviously such a compound system does not have any chance to survive against fission in the MM model. This is in a contradiction to self consistent models, according to fission barrier for neighbouring nucleus is about 12 MeV [43, 44].

Fission barriers for even-even SH elements [32] obtained within the Woods-Saxon (WS) model have characteristic maxima at $Z = 108, N = 162$ (deformed magic shells) and $Z = 114, N = 178$ (not 184). For the latter system the barrier reaches 6.34 MeV and then decreases with Z . This is in contrast with Skyrme SkM* predictions [25] of the highest barriers for $Z = 120$ [25], which is related to the proton magic gap. One has to emphasise that the barriers from the WS model are in good agreement with data for even-even actinides: for 18 first and 22 second barriers the rms deviation equals 0.5 and 0.7 MeV, respectively [32, 45].

Potential energy surfaces (PES) are often calculated and projected on the triaxial $(\beta \cos \gamma, \beta \sin \gamma)$ plane. Examples of energy maps in $(\beta \cos \gamma, \beta \sin \gamma)$ plane, necessary to evaluate fission barriers are shown in Fig. 2 (The total energy is normalised in such a way that its macroscopic part is equal zero at the spherical shape of a nucleus.)

Calculations of FRDM presented in [46] confirm aforementioned findings of the WS model e.g. region of the highest fission barrier around ^{270}Hs and $^{294}\text{Lv}_{178}$, decrease of stability between these two maxima as well as beyond $N = 184$. Nevertheless some qualitative discrepancies between two MM approaches can be found. In FRDM barriers are systematically higher by over 2 MeV. Fission barriers of odd isotopes are also calculated and discussed in the cited paper.

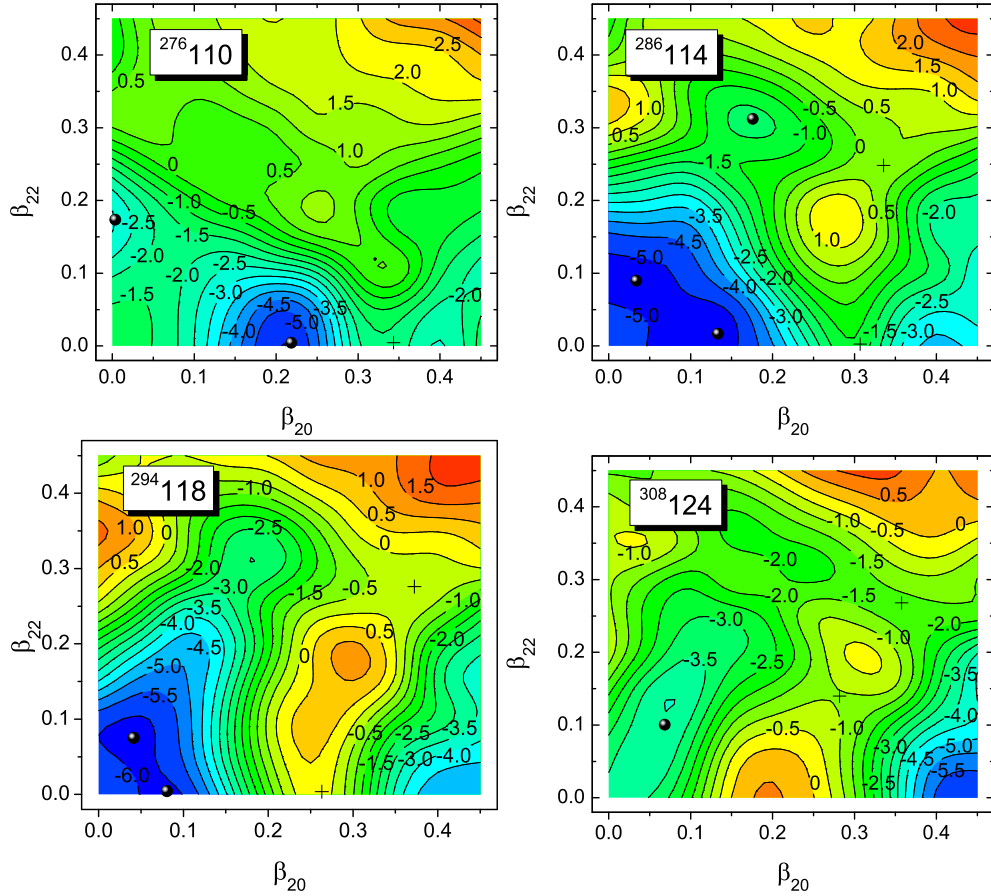


Figure 2: Energy surfaces: $E - E_{mac}(sphere)$ for the three of experimentally detected evaporation residues and one hypothetical heavier system.

2.2. Self-consistent theories

The MM methods with their two independent ingredients (LD model for bulk parameters and WS model for SP properties) lead to a rather large number of theoretically independent parameters separately fitted in LD and SP parts of the energy. Contrary to this empirical treatment, self-consistent approaches start from one density functional model for the energy of a nucleus as a whole depending on a couple of densities (local density, kinetic energy density, spin-orbit density, ...). These total energies can be generated in the HF or HFB framework from given effective interactions or modeled directly as density functionals. Such approaches exist in both regimes, non-relativistic as well as relativistic. In the following we describe the HFB approach based on two most commonly used (non-relativistic) functionals: the Skyrme type with zero-range nuclear forces and the Gogny type where the forces are of mixed nature and both zero-range and finite-range components are taken into account.

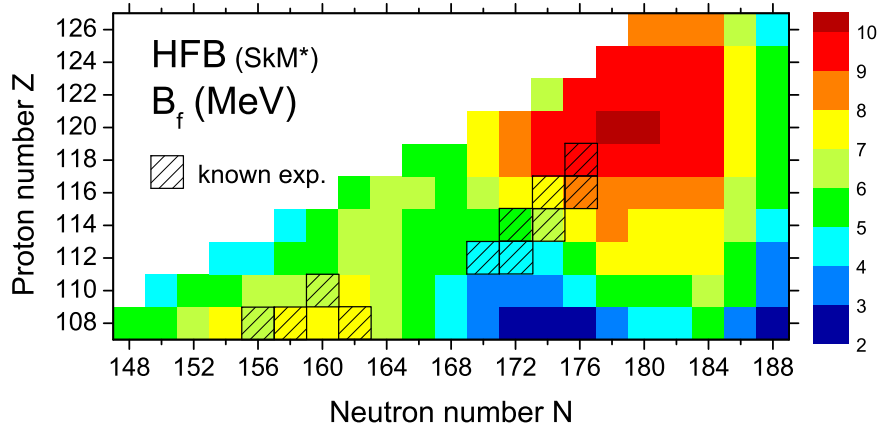


Figure 3: First fission barrier (MeV) of SH nuclei in HFB SkM* model. Cross-hatched squares represent observed nuclei.

2.2.1. Skyrme type functional

The energy in Skyrme-Hartree-Fock (SHF) or Skyrme-Hartree-Fock-Bogoliubov (SHFB) theories of nuclei reads

$$E = \int \mathcal{H}[\rho(\vec{r}), \tau(\vec{r}), \vec{J}(\vec{r}), \dots] dV, \quad (1)$$

where ρ is the local density, τ the kinetic energy density, \vec{J} the spin-orbit density, and so on. (see *e.g.*, [47, 48].)

There is a variety SHF energy density functionals which differ mainly by their parametrisations. One which is often used in the description of the fission process is SkM* [49]. Heights of the fission barriers known from experimental data and spurious rotational energies in the ground states of even-even nuclei were taken into account in the fitting procedure. Thus, fission properties should be correctly calculated.

The rather involved calculations of barriers and the fission HLs of SH elements on a global scale were possible and done only since very recently (see *e.g.*, [31, 50, 25]). The goal of the present section is to recalculate the results of previous estimates for HLs taking into account two facts: First, as it was mentioned in many places (see *e.g.*, [51, 52] where the rotational moment of inertia – a part of inertia tensor – is discussed), the Inglis cranking mass is too small in comparison to the full ATDHFB one. In this paper, we use the cranking mass but scaled with a factor 1.3 to simulate the ATDHFB mass. We follow this principle in the present section. Second, a key ingredient is the energy E_0 of the collective ground state; in earlier papers we used rather crude estimates for E_0 and in the following we use an improved semi-classical recipe (Bohr-Sommerfeld quantisation) consistent with WKB approximation which is used to calculate the tunnelling probability for spontaneous fission. Note that other calculations proceed differently in those details. For example, reference [31] used fully quantum mechanically computed E_0 without the Bohr Hamiltonian approach and the full ATDHF masses. Figure 3 shows the systematics of the barrier heights calculated with SkM* in the region of $Z = 108(2)126$ and $N = 148(2)188$. In the experimentally known region, the barriers are of the order of 6-7 MeV. The barriers of heaviest nuclei are relatively high and reach 8-10 MeV. From the point of view of the barrier height the most stable nuclei with respect to fission decay are close to $Z = 120 - 122$ and $N = 178 - 180$. There is a region of low barriers height near the line $A = 282$. This would

predict a valley of fission instability in this particular region of superheavies. On the other hand there is experimental evidence [53] which contradicts calculations.

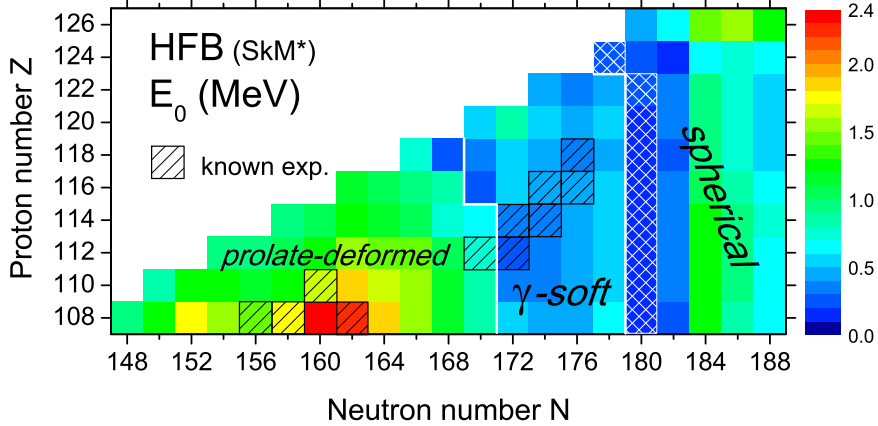


Figure 4: Ground state energies from WKB quantisation rule (see Eq. 2). Different deformation regions: prolate, γ -soft and spherical are approximately depicted. Cross-hatched squares represent observed nuclei.

The calculation of main ingredients of the theory, namely the PES and the collective mass parameter were described elsewhere [28, 25]. We map the deformation landscape by adding a quadrupole constraint stretching the system successively to scission. The PES is then obtained as a function of the mass quadrupole moment defined as the average value of the quadrupole operator $q_2 = \langle \hat{Q}_{20} \rangle = \langle \sum_{i=1}^A (2z_i^2 - x_i^2 - y_i^2) \rangle$. Two further constraints, namely the triaxiality and reflection asymmetry, were applied in the region of the first barrier and beyond. A detailed discussion is given in [25, 28]. Here we only discuss some new aspects concerning the spontaneous fission process.

The ground state energy measured relatively to the minimum of the potential energy is crucial in determining the HLs of the nucleus with respect to fission. The approximate fission probability P stemming from WKB theory involves mass parameters B , potential energy V and the energy of the collective ground state of the system E_0 . The requirement that the phases of WKB functions coincide (modulo $n\pi$) in the region of their overlap leads to the quantization condition. Then the following relation between the quantities involved should be fulfilled for a stationary state [54]

$$S_{ab} = (n + 1/2)\pi, \quad (2)$$

where, in general, the action S_{ab} (in units of \hbar) calculated between two points a and b is

$$S_{ab}(E_0) = \int_a^b \sqrt{2B(q)[E_0 - V(q)]} dq. \quad (3)$$

The coordinate q is the leading collective coordinate towards fission (*e.g.*, $q = \langle \hat{Q}_{20} \rangle$ or $q = \beta$), $n = 0, 1, 2$ etc. In Eq. 2 a and b are the classical turning points determined from the equation $V(q) = E_0$ solved in the vicinity of the ground state. The Eq. (3) is similar to the Bohr-Sommerfeld quantisation rule (see *e.g.*, [55]). It can be easily solved for each considered nucleus with respect to E_0 . While the fission probability P strongly depends on E_0 the results of calculation will be different from those where one assumes a constant $E_0 = 0.5$ MeV for all nuclei (see

e.g. [56, 51]) or quantum mechanically exact values [31]. The values of the ground state energies E_0 calculated from the Eq. 2 are shown in Figure 4. It is interesting to observe correlations of this quantity with the corresponding ground state deformations [57].

For the mass parameter we aim at the adiabatic time dependent HFB (ATDHFB) cranking approximation. As it was already mentioned, the Inglis cranking mass parameters are on the average smaller than full ATDHFB ones. Therefore to do more realistic calculations of fission HLs we assumed according to other authors the scaled fission mass tensor component. The scaling factor 1.3 was applied. This leads in general to larger values of E_0 [see Eq. (3)] but HL remains the same as mass parameters are larger.

The next Figure 5 shows the fission HLs calculated in this way with SkM* parameter set.

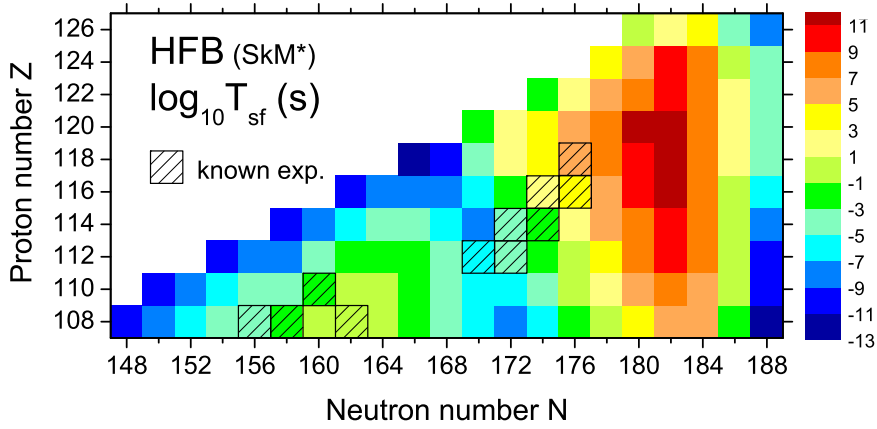


Figure 5: Fission HLs (sec) of superheavy nuclei in microscopic HFB SkM* model. Cross-hatched squares represent observed nuclei.

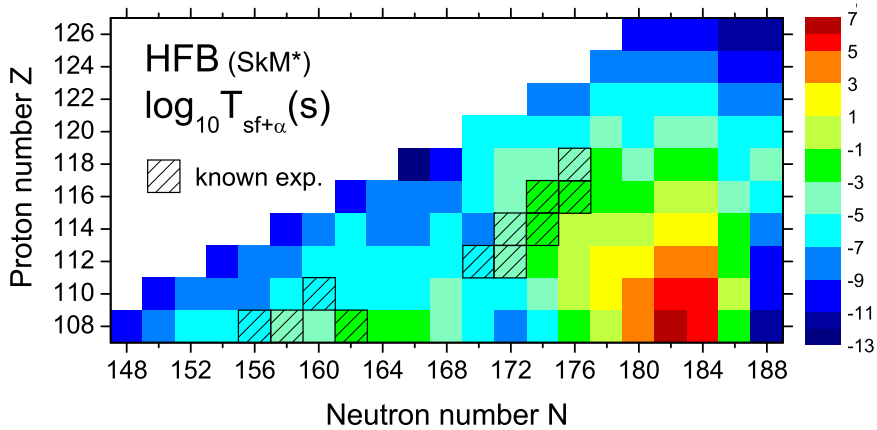


Figure 6: Total HLs (fission + α) of superheavy nuclei in HFB SkM* model. Cross-hatched squares represent observed nuclei.

The WKB quantisation rule which delivers the ground state energy E_0 for fission works well at

least in the region of known elements as e.g., in the case of fermium isotopes [58]. Its extrapolation to SH elements seems to be better than an *ad hoc* procedure which was assumed previously where the ground state energy E_0 was equal to $0.7 E_{ZPE}$ where E_{ZPE} is zero point energy, or it is a constant equal to 0.5 MeV.

After taking the α -decay into considerations the HLs for some nuclei change substantially. To estimate α -decay half-lives, we used the standard Viola-Seaborg expression [59] with the parameters from Ref. [60]. The resulting HLs are shown in Figure 6. According to our calculations the longest total HLs correspond to nuclei in the vicinity of $Z = 112$ and $N = 182, 184$. The region of most stable nuclei is located in the vicinity of $Z \sim 112, N \sim 182, 184$ [25]. It is worth

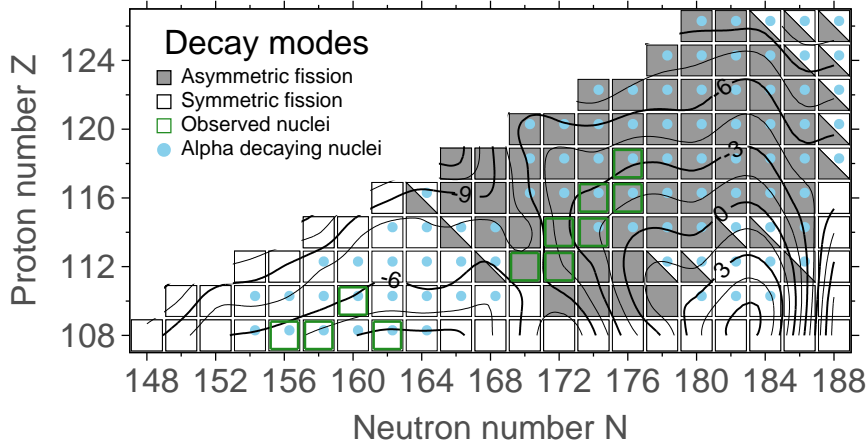


Figure 7: Regions of symmetrically and asymmetrically fissioning nuclei in HFB SkM* model. The filled circles (blue) represent nuclei decaying mainly by alpha emission. The isolines show approximate total HLs (in seconds). Experimentally registered nuclei are depicted as thick (green) squares.

to mention the existence of two main modes of fission. The symmetric mode (the same spherical fragments) which dominates in the region of light SH nuclei and the asymmetric one prevail in the region of still heavier systems. Both symmetry regions are shown in the Figure 7. The separation line is close to $A \sim 280$. The asymmetric fission region is concentrated at $Z \sim 118$ and $N \sim 178$. It is observed that the heaviest nuclei ($N > 186$) decays probably in the asymmetric way. The thick squares shown in Figure 7 correspond to nuclei for which experimental data for fission and/or alpha decay HLs are known [53]. These trends are in agreement with the survey of [50] using a couple of other Skyrme parametrisations.

Fission barrier heights and HLs with respect to spontaneous fission as obtained from self-consistent HFB SkM* calculations differ considerably from the ones presented in the previous section where MM models were used. The main difference are the barriers. They are usually higher in the case of HFB SkM* model up to 2-3 MeV at some cases. This feature is common for all non-relativistic self-consistent approaches.

There are of course discrepancies between the theoretical and the experimental data, the largest ones in the region of the middle mass SHE. Since those systems belong to the region of shape coexistence some further increase of spontaneous fission HLs is anticipated due to shape mixing. In order to improve upon the theory of fission we shall consider the inclusion of several collective coordinates and the dynamics of spontaneous fission process, the improved energy

density functionals [61], and the full ATDHFB inertia parameters. The work is in progress. Some introductory results have been already published [29].

2.2.2. *The Gogny functional*

The Gogny force [62] is a non-relativistic effective phenomenological interaction widely used to describe the low energy dynamics of the atomic nucleus. It is intended to be applicable to all possible nuclei from drip line to drip line using a limited set of parameters adjusted to global properties. In addition to the standard central, spin-orbit and Coulomb potentials it contains a phenomenological density dependent term depending on the density raised to the power $\gamma = 1/3$ introduced to incorporate the saturation mechanism of nuclear forces. In many aspects, it is similar to the Skyrme [63] interaction sharing with it the spin-orbit potential, Coulomb and the idea of a density dependent repulsive part. However, Skyrme's zero range and gradient terms present in the central potential are replaced in the Gogny force by a finite range potential linear combination of two gaussians. The main advantage of the finite range is that the corresponding matrix elements are free from ultraviolet divergences allowing the treatment of the particle-particle (pairing) channel with the same interaction.

In most of the fission studies carried out with the Gogny force, the focus has been in the characterisation of just one of the fission observables, namely the spontaneous fission lifetimes (or derived quantities like fission barrier heights and widths) in even-even nuclei. Studies aimed at the description of induced fission in the framework of finite temperature HFB are scarce [64] and deserve more attention. This is the same as with fission in odd mass nuclei where the understanding of the specialisation energy is of fundamental interest. In this respect, there is only one example with the Gogny force [65]. Recent advances in the experimental techniques allow for the study of the evolution of fission parameters with spin [66]. The expected decrease of the barrier height with spin and the evolution of triaxiality in the first barrier has been studied with the Gogny force in Ref [67].

At this point, it has to be mentioned that the ability of any of the Gogny parametrisations to reproduce fission observables (mainly spontaneous fission HLs) is spoiled by the strong dependence of those quantities with the value of the collective inertia in the forbidden region. As the collective inertia strongly depends on the pairing gap as the inverse of its square it is to be expected that pairing properties should play a central role in the theoretical description of fission. In this respect, we can mention two studies [68, 69] with D1S, D1N and D1M where the spontaneous fission lifetimes of the neutron rich uranium and plutonium isotopes have been considered. The variation of the HLs with the pairing strength was found to be enormous in absolute value although the trend with neutron number was roughly preserved. As a consequence of this variability, the results also depend upon the principles involved in the determination of the path to fission. The recent results of [70] using the minimum action principle with pairing degrees of freedom are markedly different from those using the minimum energy principle (*see* Section 3.2). The reason again is the strong dependence of the collective inertia on the pairing gap (it goes as the inverse of the square of the pairing gap) that has a strong impact on the action.

The PES calculated in a microscopic model like HFB theory provide a lot of information on the fission properties of SH elements. HLs, preferred decay channels and fission types (symmetric, asymmetric, highly asymmetric) can be deduced by the analysis of PESes. As it was mentioned above, results derived within HFB theory are obtained with some systematic theoretical errors (*see* Section 4). Nevertheless, it is reasonable to compare results between particular isotopes and distinguish groups of nuclides with specific decay properties. An early study of SH region in the HFB model has been performed by Bruyères-le-Châtel group in [71, 72, 73, 74, 75]

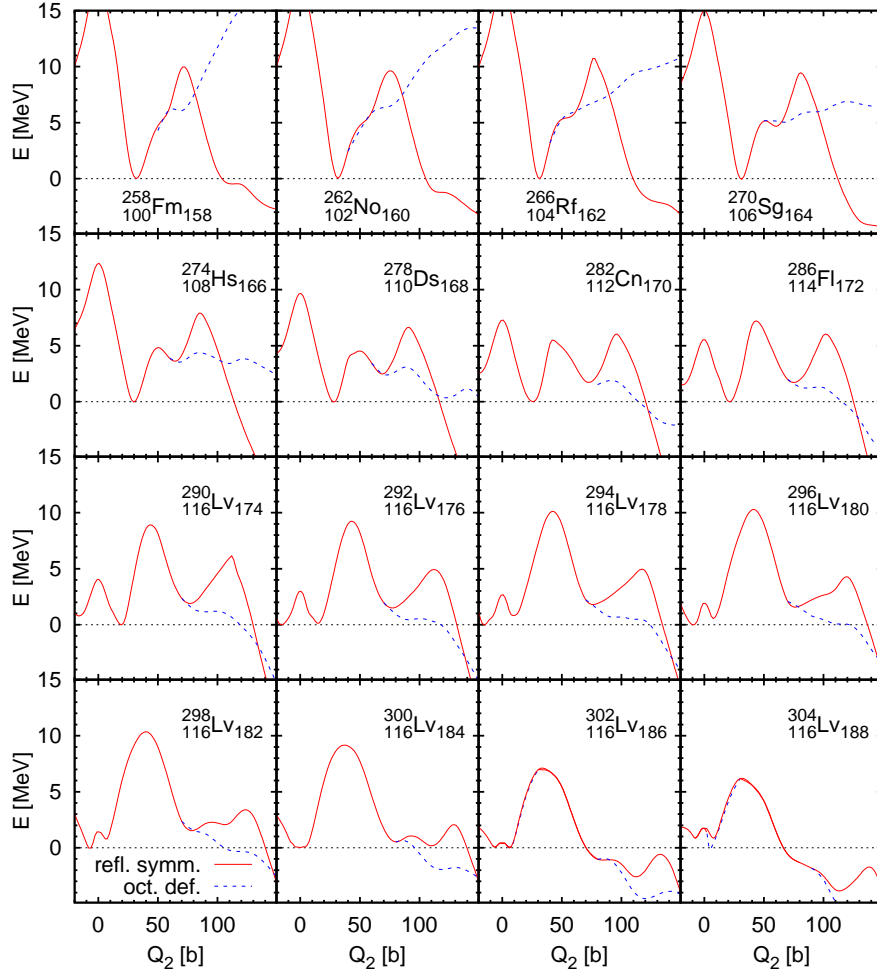


Figure 8: Axial fission barriers of selected isotopes across the SH nuclei. Note that in the original paper [24] the quadrupole moment Q_2 was a factor of two smaller.

and Lublin-Madrid group in [76]. The most thorough investigation using the D1S Gogny interaction in the axial symmetry regime has been published in [24]. Details of the method are described in [51].

Fission characteristics are determined not only by the height of the fission barrier but also by its shape and localisation in the deformation space. From the general overview of the fission barrier shapes across the SH nuclei one can find that the number of protons affects mainly the height of the barrier whereas substantial changes of the barrier profile take place along isotopic chains. In consequence, fission properties depend mostly on neutron number. Selected fission barriers of SH isotopes calculated in the axial regime are presented in Fig. 8.

The lightest SH elements, with neutron number below $N = 170$, are well prolate deformed in the ground state. The saddle point in these nuclei has very high energy, often exceeding 8

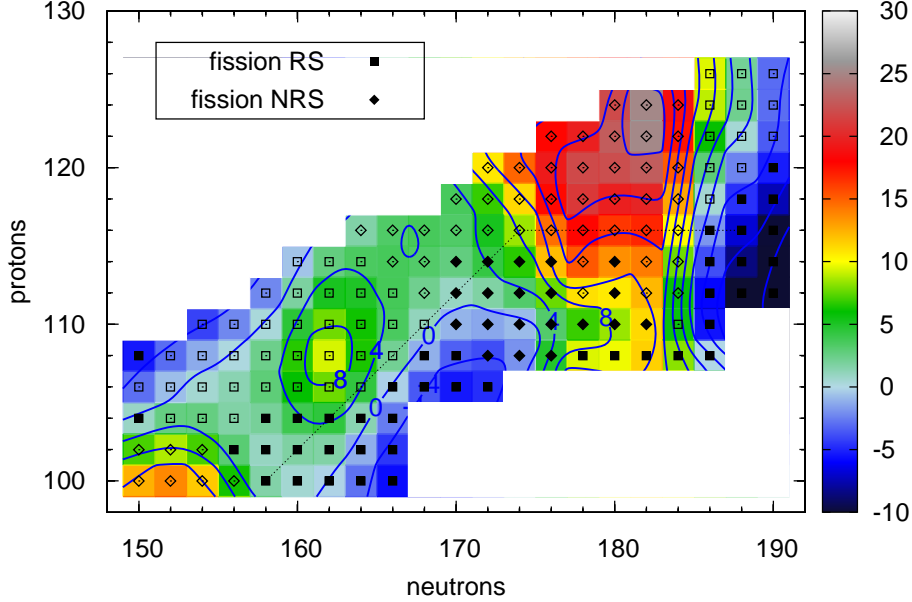


Figure 9: Logarithm of the spontaneous fission HLs in seconds computed with the HFB model and the DIS Gogny force. Nuclides with dominant fission are represented by filled symbols whereas those with dominant α decay are marked by open symbols. Dotted line indicates isotopes which fission barrier is presented in Fig. 8.

MeV. Going along any isotopic chain in this region from $N = 150$ to $N = 162$ one can observe increasing width of the fission barrier while the barrier height remains almost unchanged. As a consequence, the action integral across the barrier increases and longer HLs are observed (see Fig. 9). The centre of the region of extended stability is predicted for ^{270}Hs with the longest fission HL $\log(t_{\text{SF}}/\text{s}) = 12.83$. The corresponding nucleon numbers, namely $N = 162$ and $Z = 108$, are sometimes called “deformed magic numbers”. The special characteristics of the $N = 162$ and $Z = 108$ system are correlated with the decrease of the neutron pairing energy in the ground state and a small value of the proton one [24]. This is consistent with the aforementioned MM and Skyrme model results.

In most of the isotopes below $N = 162$, the fission barrier goes through reflection symmetric shapes. Only in the nuclei in the transitional region between the actinides and the SH elements with $A \sim 250$ octupole shapes play an important role in the determination of the fission barrier height. The reflection symmetric character of the barriers brings about symmetric fragment mass distribution in this region. The barrier height may be reduced by a few MeV in the whole region if non-axial deformations are included in the calculations [51].

Beyond $N = 158$, we find several different trends in the structure of the PES. First, the top of the fission barrier splits into two peaks: the first one is lower and the second one higher. In isotopes heavier than $N = 162$ the height of both saddles decreases and, in consequence, HLs of subsequent isotopes become shorter. The second, reflection symmetric saddle may be additionally diminished if other degrees of freedom characterising the nuclear shape are allowed. Octupole deformation cuts off the second barrier, but up to $A = 280$ such reflection asymmetric barriers extends to large quadrupole deformations and can not become the dominant fission

channel. In heavier nuclides the width of the octupole deformed hump in the fission path is comparable to the reflection symmetric one and asymmetric fission can be observed as a dominant fission channel. Also triaxial shapes can decrease the height of the second barrier but at the cost of increasing the inertia and therefore the contribution to the action remains unchanged [24].

In the same range of neutron numbers, the ground state deformation decreases and energy difference between prolate and oblate minimum reduces. In isotopes with $178 \leq N \leq 182$ the oblate minimum becomes the ground state. When non-axial deformations are taken into account, the local minimum with higher energy becomes a saddle point and there is a path along the γ plane connecting it with the ground state.

As a consequence of the aforementioned changes of the PESs, fission HLs decrease with the mass of nuclides. Minimal values, not longer than $t_{\text{SF}} = 10^3$ s, are reached around neutron number $N = 170$ in each SH element.

The first peak of the barrier keeps the axial reflection symmetric character in the whole region above $N = 158$. Its height shows a growing trend with both neutron and proton number in isotopes between $N = 170$ and $N = 182$ which is responsible for increasing fission HLs up to $N = 182$. The isotopes with two neutrons more ($N = 184$) have got features of magic nuclei: well pronounced spherical ground state with small pairing energy and large shell gap in neutron single-particle energy spectrum. However, a lower fission barrier induces here larger fission probability than in lighter isotopes. There is no strong indication of magic character of any proton number in this region of SH elements in the calculations with the Gogny force.

Beyond $N = 184$ the second, octupole deformed barrier drops away below the ground state energy level and fission barrier becomes substantially narrower. This change dramatically reduces fission HLs by several orders of magnitude with adding subsequent pair of neutrons. On the other hand, in the nuclei with neutron number greater than $N = 184$ octupole deformation decreases the ground state energy by a varying amount that can reach the 2 MeV. This decreasing of the ground state energy work in the direction of increasing again the height of the fission barrier. However, this effect is not strong enough as to counteract the above mentioned reduction of the fission HLs.

Two regions of extended stability against fission can be found in the SH elements, see Fig. 9. The first is around the deformed magic nucleus ^{270}Hs where fission HLs reach the level of 10^{12} s. The second region covers isotopes with neutron number $N = 182$. The HLs in elements with large proton number reach here much larger values extending far above $t_{\text{SF}} = 10^{20}$ s. It is important to notice the lower stability against fission in isotopes around $N = 170$ which is presently in the focus of experimental investigations. In nuclei heavier than $N = 186$, a decrease of potential energy with deformation dictated by LD bulk properties dominates over the stabilising shell correction. High fission barrier can thus not be achieved and the fission stability drops rapidly.

The main decay process competing with spontaneous fission in SH elements is α radioactivity. The predicted α decay HLs are shorter than fission ones in proton rich isotones. Thus, it can be noticed that fission is the dominant decay channel in three regions [24]. First, in the vicinity of deformed magic nucleus ^{270}Hs symmetric fission can be found. Second, asymmetric fission is dominant for nuclei elements lighter than Fl ($Z = 114$) and below magic neutron number $N = 184$. Finally, for heavy isotopes with $N \geq 186$ and $Z \leq 118$ again symmetric fission occurs with very short HLs.

In those isotopes beyond $N = 190$, the macroscopic part of the nuclear potential makes fission barriers too small to allow for sufficiently long HLs that could be detected experimentally. The existence of heavier nuclei is possible only in exotic ground state configurations. Bubble nuclei,

spherical symmetric systems, without nuclear matter in the centre, are predicted for charges $Z \geq 240$ and masses $A \geq 700$ [71, 72, 73, 74, 75]. Lighter nuclei with $Z \geq 170$ and $A \geq 450$ can exist in semi-bubble configuration where central density is reduced to half of the bulk nuclear matter density. Another type of exotic shape that may exist beyond SH nuclei is the one of a torus [77]. The HFB theory with Gogny force predicts a toroidal structure with energy lower than spherical configuration for nuclei with $Z > 140$. The stability of such exotic shapes is questionable and it has to be confirmed in further investigations.

2.2.3. Relativistic Mean Field

Fission barriers in SH nuclei has been also investigated in covariant density functional theory [36]. Modern parametrisation DD-ME2 and DD-PC1 was used together with modified version of traditional NL3*. It was found that both triaxiality and octupole deformation substantially affect the second barrier in nuclei with $Z \geq 112$. It was found that the first barrier remains axially symmetric in the whole region.

Triaxial deformation decrease energy of the saddle point as much as 3 MeV in some isotopes with $N < 174$. The NL3* and DD-ME2 predict the lowest saddle point energies among the all models of nuclear forces. The DD-PC1 parametrisation gives slightly larger values.

2.3. Mass parameters and their impact on half-live times

The collective mass along the fission path influences the fission HLs with the same importance as the barrier does. This can be seen from formula (3) for the action integral where the mass $B(q)$ and the potential energy $V(q)$ enter the action as a product. A relatively recent discussion of the mass tensor calculations can be found in [28].

Mass parameters are usually calculated within perturbative cranking approximation (or Inglis inertia) or adiabatic time dependent HF or HFB model where one differentiates the fields of the model numerically instead (see, *e.g.*, [78, 52, 51, 31, 79, 80]).

The shapes of the mass tensor components are fairly similar in both mentioned cases but the values of specific components differ substantially. The simple cranking masses calculated in *e.g.*, one dimensional space are usually smaller then ATDHF cranking masses. This influences, in turn, the fission HLs. In the EDF of the Gogny type models of nuclear structure where the barriers are much higher then ones from *e.g.*, MM or RMF models, these small masses lead to smaller HLs, which sometimes coincide with experimental ones. On the other hand, the Skyrme EDF give smaller barriers then Gogny ones and the ATDHF cranking masses are numerically calculated. They generate HLs much larger or comparable to that of the Gogny model. In the MM models the barriers are believed to fit rather well experimental data and one uses the simple perturbative cranking approximation for the masses. Unfortunately that leads to too small (in comparison with experiment) HL times. The other feature is the collective inertias strongly depend upon the pairing strength what makes the pairing degree of freedom an important ingredient (see the section on dynamics of fission (3.2)).

The above discussion shows that there is still a multitude of different approaches to compute the collective mass along the fission path. This hinders a direct comparison of the final fission HL. It is a challenge for the future projects to remove all of these differences in the calculations of the nuclear inertia by adopting the same ATDHF cranking model everywhere. Only then it will be possible to judge the models and the validity of the barrier heights as well as the validity of final HL.

3. Comparison of calculated fission barriers to experimental data

There are two main methods of calculating fission HLs and barriers, namely the static method (minimisation of the potential energy and extraction of the saddle points) and dynamic (minimisation of the action integral). Most of the calculations (and these in this paper) concerning fission barriers are of the static type.

3.1. Static fission barriers

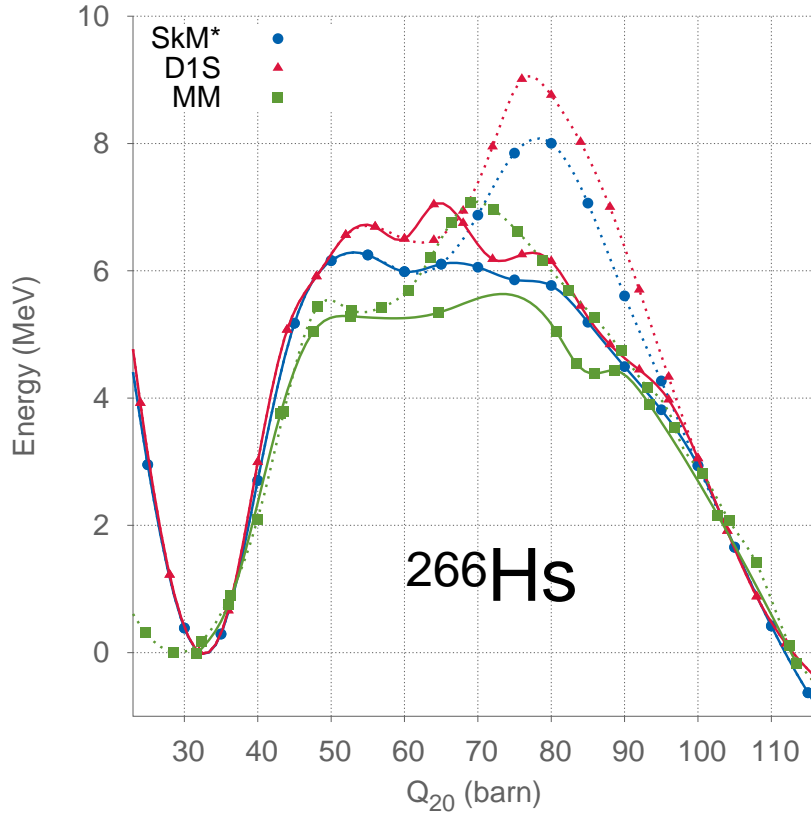


Figure 10: Fission barriers of ^{266}Hs as functions of the quadrupole moment Q_{20} calculated in MM model (green, filled squares), Skyrme HFB approach (blue, filled circles) and Gogny HF model (red, filled triangles). Dashed lines represent the raw axial barrier. Solid lines correspond to the barriers with γ . The values of Q_{20} for MM curves are close to the actual, but not completely accurate.

We start with the comparison of the fission barriers for ^{266}Hs as an example of mid-mass SH isotope calculated in models discussed in the paper. The barriers derived in the MM, Skyrme HFB and Gogny HF models are shown in Fig. 10 as functions of quadrupole moment Q_{20} . The shapes of all PES are very similar and there is relatively good agreement of barrier heights. The differences in the peak height (the saddle point) reach 1 MeV. Rather small differences remaining are hard to explain because the models are very different in their structure. The differences shown will weakly impact on calculated fission HLs. Fig. 11 shows four sets of calculated fis-

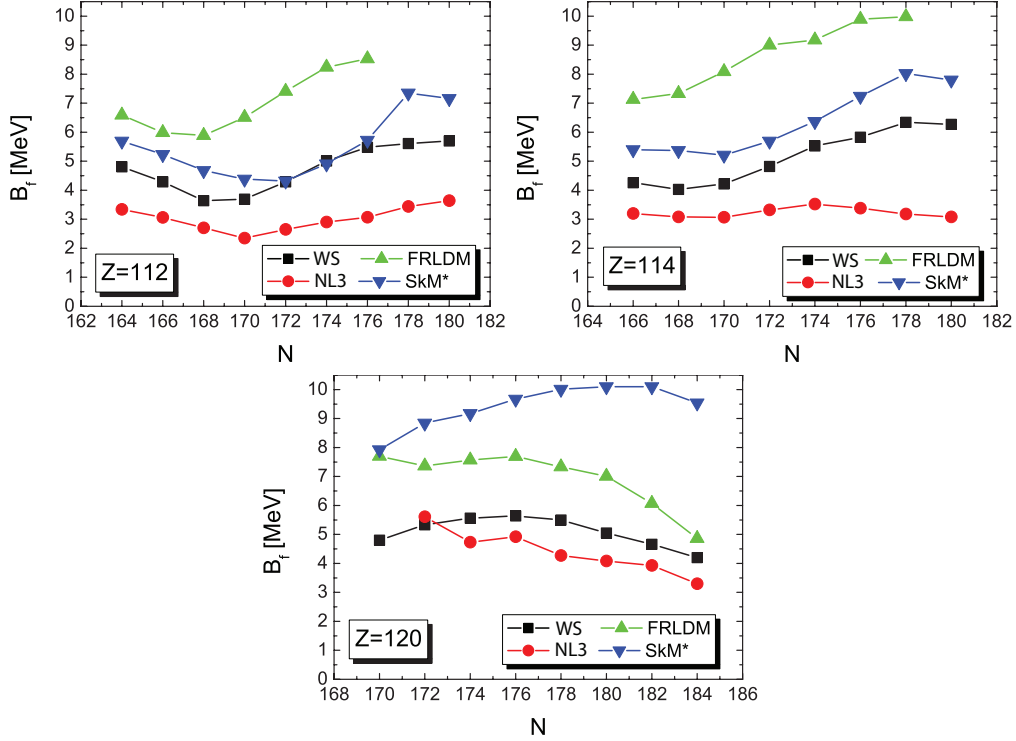


Figure 11: Fission barriers predicted by various models: black - WS model [32], green - FRLDM [35], blue - SkM* [25], red - RMF with NL3 parametrisation [36].

sion barriers B_f for even-even isotopes of $Z = 112, 114$ and 120 : from the WS model [32], the macroscopic-microscopic Finite Range Liquid Drop Model (FRLDM) [35], HFB calculations with the SkM* interaction [25] and the RMF model with NL3 parametrisation [36]. Results of rather comprehensive calculations were selected: all were made for dozens of nuclei and included important triaxial and mass-asymmetric deformations. One has to emphasise that three of those models well reproduce experimental barriers in even-even actinides; the SkM* model overestimates actinide barriers by 1-2 MeV. In spite of this, the differences in predictions in Fig. 11 are conspicuous. In order to quantify this, we refer to the known spontaneous fission (s.f.) HLs: 0.8 ms in ^{282}Ds , 97 ms in ^{284}Ds and 130 ms in ^{286}Fl . The values predicted some time ago [81] from the sub-barrier action minimisation based on the WS model were, respectively, 71 ms, 4 s and 1.5 s (1-2 orders of magnitude overestimate; only axial deformations were included in [81], but axially symmetric shapes at the barrier in these nuclei were actually confirmed in [32]). One can observe that the FRLDM barriers for $Z = 112, 114$ are much higher than in the WS model and could hardly produce HLs in agreement with experiment. As we have checked, this huge difference in barriers in the two MM models is not related to shape parametrisation. The spontaneous fission HLs for the three nuclei calculated in [25] along static path (no action minimisation) are (surprisingly, in view of barriers similar to ours) by many orders of magnitude too short. On the other hand, RMF calculations [36] produced barriers much lower than in the WS model which could hardly explain the measured evaporation residue cross-sections in fusion.

In Table 1 we collect some of the theoretical predictions of fission barrier heights based on the FRLDM [35], SHF – self consistent Hartre-Fock method [82] with the SLy6 Skyrme interaction [83] and the Extended Thomas-Fermi plus Strutinsky Integral model (ETFSI) based on Skyrme SkSC4 functional [84] in relation to experimental ones [85] and our predictions in a MM and SHFB(SkM*) models. Note that the lower limits for the fission barrier heights are evaluated in Ref. [85]. As we can see, experimental and MM calculated barrier heights are in agreement while FRLDM, SHF and SHFB generally overestimate the barrier heights. Surprisingly the modern version of the MM calculation presented in Ref. [35] (including nonaxial shapes) gives values comparable to axially-symmetrical calculations of SHF and overestimate the experimental barriers in a similar way. This tendency is visible, to a lesser extent, also for heavier systems. Thus for the isotope $^{292}\text{Ds}_{176}$ the FRLDM model gives a value of 9.25 MeV for the barrier height while the value obtained in our approach (6.22 MeV) is about 3 MeV lower, whereas the experimental data indicate 6.4 MeV. For the neighbouring isotope $^{292}\text{Lv}_{178}$ the experimentally predicted fission barrier is also 6.4 MeV and we obtain also almost the same value 6.28 MeV, but estimations based on the FRLDM predict a value of 9.46 MeV, almost 3 MeV larger. As a consequence, such high barriers result in cross sections for $Z=114, 116, 118$ and 120 which overestimate the experimental data by several orders of magnitude [86, 87]. The ETFSI(SkSC4) model significantly underestimates the barrier heights for $^{284}\text{Cn}_{172}$ and $^{286}\text{Cn}_{174}$ for heavier systems the agreement is however much better. One must keep in mind that ETFSI(SkSC4) and SHF(SLy6) models do not include triaxial nor higher order nonaxial degrees of freedom and the observed discrepancies probably can be explained by the absence of these variables at the saddle point configuration.

3.2. Fission dynamics

As it was shown years ago [88, 89] and also in recent publications [29, 30, 68, 90] the minimisation of the reduced action integral instead of the potential energy leads to larger fission probabilities or equivalently to shorter fission HLs. The latter are generally reduced by one to two orders of magnitude in comparison to statically calculated HLs. At the same time, the calculated fission barriers increase by 1-2 MeV. While these kinds of calculations are rather involved, one usually performs static calculations of HLs integrating the action along the potential energy valley leading to the fission of the nucleus. This is common to all calculations.

The dynamic treatment of some internal degrees of freedom like *e.g.*, pairing gap (*see* [91] and the very recent paper [70]) or particle number fluctuation parameter λ_2 in Lipkin-Nogami pairing model [68, 29, 30] seems to be more significant than a similar treatment of space-type deformation coordinates described above. While the latter is already well known to be similar for all instances the former depends on the considered nucleus. For a few cases, it was shown in the above cited papers that a dynamical treatment of the pairing field is important and one should include pairing fluctuations as a dynamical variable in the calculation of HLs. The dynamical change of *e.g.*, the pairing gap being the consequence of action minimisation corresponds to the fission path on which the collective mass parameter is generally smaller than one on the static pathway and at the same time the fission barrier increases as compared to the static one. The final HL is reduced again. The reduction factor is around one order of magnitude. For reasons of space, we do not discuss this type of calculations in detail here.

Table 1: Comparison of fission barrier heights with another theoretical evaluations: SHF(SLy6) [82], SHFB(SkM*) – this paper, FRLDM [35], ETFSI(SkSC4) with Skyrme SkSC4 force [84], WS [32] – present paper, and experimental data taken from [85].

Nucleus	SHF (SLy6)	SHFB (SkM*)	FRLDM	ETFSI (SkSC4)	WS	EXP
²⁸⁴ 112 ₁₇₂	6.06	4.31	7.41	2.2	4.29	5.5
²⁸⁶ 112 ₁₇₄	6.91	4.74	8.24	3.6	5.01	5.5
²⁸⁸ 114 ₁₇₄	8.12	6.24	9.18	6.1	5.53	6.7
²⁹⁰ 114 ₁₇₆	8.52	7.13	9.89	6.6	5.83	6.7
²⁹² 114 ₁₇₈	-	8.14	9.98	7.2	6.34	6.7
²⁹² 116 ₁₇₆	9.35	8.72	9.26	6.5	6.22	6.4
²⁹⁴ 116 ₁₇₈	9.59	8.84	9.46	7.2	6.28	6.4
²⁹⁶ 116 ₁₈₀	-	8.54	9.10	7.2	6.07	6.4
²⁹⁴ 118 ₁₇₆	-	9.19	8.48	6.6	5.99	-
²⁹⁶ 118 ₁₇₈	-	9.47	8.36	7.0	6.04	-
²⁹⁸ 118 ₁₈₀	-	9.28	8.05	7.4	5.72	-
²⁹⁶ 120 ₁₇₆	-	9.48	7.69	6.2	5.64	-
²⁹⁸ 120 ₁₇₈	-	10.05	7.33	6.6	5.50	-
³⁰⁰ 120 ₁₈₀	-	9.91	7.01	6.8	5.05	-
³⁰² 120 ₁₈₂	-	9.82	6.07	7.2	4.66	-
³⁰⁴ 120 ₁₈₄	-	9.54	4.86	6.8	4.20	-

4. Uncertainties on barriers and correlations with other observables

So far, we have mostly presented the results for the various models separately. A direct comparison of barriers for four selected models was done in Figure 11 and it shows that the predictions on fission properties can vary widely amongst the models. It is the aim of this section to explore the variations of predictions on a broader and more systematic basis. To this end, we will exploit statistical analysis built on least-squares techniques for optimising parametrisation. We will briefly summarise the least-squares techniques, then discuss the various influences on barriers by explicit variation of force parameters, and finally present systematics of extrapolation uncertainties and correlations with system properties from statistical analysis. The basic principles of χ^2 error estimates and correlations analysis have been explained in great detail in [92]. A practical application in the context of SHF with inspecting a broad range of observables is found in [93]. Following the scope of this paper, we concentrate here on fission properties. As we have seen in figure 11 that the isotopic and isotonic trends of fission properties are about the same for the different models, we confine the study to one representative test case, fission properties of ²⁶⁶Hs as a prototype super-heavy element.

4.1. The fission path of ²⁶⁶Hs

The fission path is a set of mean-field states $|\Phi_q\rangle$ comprising a range of relevant quadrupole deformations q . In self-consistent mean-field models, it is generated by mean-field calculations with quadrupole constraint, see *e.g.* [78]. This yields the potential-energy surface (PES) for fission. Figure 12 shows the PES for our test case ²⁶⁶Hs. It is what we call the “raw PES” which

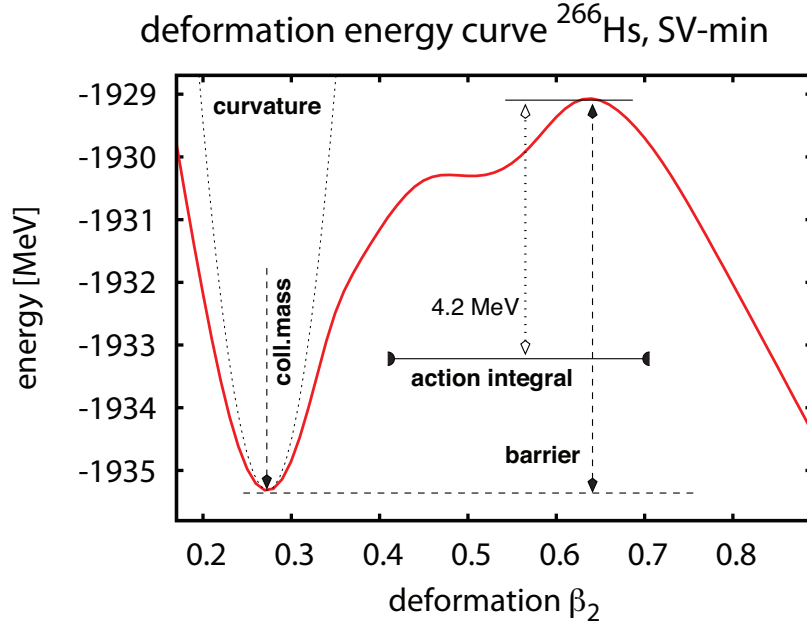


Figure 12: Illustration of the potential-energy surface (PES) along the axially symmetric fission path of ^{266}Hs and its four key quantities: curvature of the PES at the ground state, fission barrier, mass parameter B at the ground state, and the action integral $= \int_{0.4}^{0.7} d\beta_2 \sqrt{B(V_{\text{PES}} - E_{\text{sub}})}$ with $E_{\text{sub}} = V_{\text{max}} - 4.2\text{MeV}$ as appropriate average quantities in the tunnelling regime. The PES was computed with quadrupole constrained SHF calculations using the parametrisation SV-min.

emerges as expectation value of energy for given deformation. The actual fission calculations will invoke also the mass parameter along the path and augments the raw PES with quantum corrections (zero-point energies) [78, 31]. This modifies the PES and with it the barriers. Fortunately, the modifications are moderate for ^{266}Hs . This allows us to confine the discussion of trends and correlations to properties of the raw PES. For simplicity, we will also confine the considerations to the fission path along axially symmetric shapes. It is known that triaxiality produces for ^{266}Hs typically about 1 - 2 MeV lower barriers (cf. Sec. 3.1 and Fig. 10). However, axial shapes suffice for the purpose of comparing different parametrisation and studying trends and correlations.

For a systematic analysis, it is advantageous to reduce the information on the PES to a few key quantities. Figure 12 illustrates the choice of these key observables. The most obvious quantity is the height of the fission barrier B_f . In the following we consider B_f as a difference between the saddle point of PES and the energy of mean-field ground state. (Note that the effective barrier seen in experiment is rather the difference between the saddle point energy and the collective ground-state energy which lies typically 1-2 MeV above the mean-field ground state energy.) The collective ground state is characterised by the curvature $\partial^2 E(q)/\partial q^2|_{q_{\text{min}}}$ and the mass parameter (not shown here) at the minimum. Another key piece for determining fission HL is the WKB action integral (see Eq. 3) for tunnelling. This is a very involved quantity as it depends on entry and exit point for the tunnelling regime which, in turn, depend sensitively on the energy of the collective ground state. We want here a simpler measure concentrating on the

mass parameter in the tunnelling regime. As this parameter varies considerably along the path (see figure 14) we consider an average taken over the core of the tunnelling regime. To that end, we consider the action integral S (see caption) in the form as it enters the tunnelling integral. In order to concentrate on the effect of the mass $B(q)$, we confine the integration regime safely inside the turning points and take a fixed energy of 4.2 MeV. Of course, the actual value for the action integral depends on this reference energy. But we are interested in comparing differences which develop when varying the forces. The trends seen in such variations are the robust against the detailed choice of reference energy and integration limits.

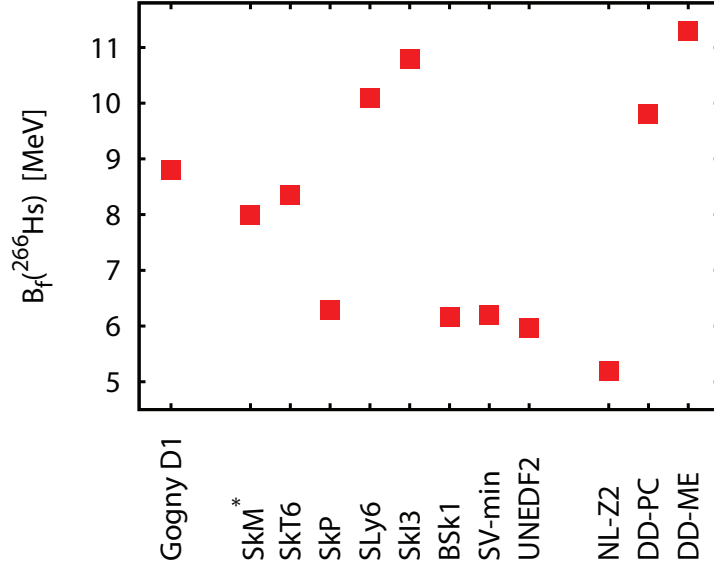


Figure 13: The axially symmetric fission barrier of ^{266}Hs for a great variety of published models and parametrisation. The basic citations for the models and parametrisation are: Gogny [94], SkM* [49], SkP [95], SkT6 [96], SLy6 [97], SkI3 [98], BSk1 [99], SV-min [100], UNEDF2 [101], NL-Z2 [102], DD-PC and DD-ME [103].

Before proceeding to χ^2 analysis, we illustrate in figure 13 the broad span of predictions for the most important quantity of the fission path, the fission barrier of ^{266}Hs . To that end, we have fetched a couple of published parametrisation from early first generation models to latest developments. There are three formally different models involved, the Gogny force to the left, a large group from SHF in the middle, and three RMF models at the right. Even within one model family, SHF or RMF, one sees a large variation of results and it is obvious from this figure that many of the parametrisation have to be ruled out for fission calculations. For SHF we can establish a trend of B_f with the effective mass m^*/m of a parametrisation where low m^*/m is related to large B_f and vice versa. This argument does not apply to the three RMF parametrisation which all have about the same low m^*/m . Here it is a strongly varying incompressibility K which causes the different B_f . After all, the example of figure 13 demonstrates that an arbitrary collection of parametrisations does not allow to conclude unambiguously on the relations between properties of a force and predicted observables (here B_f). Statistical analysis based on χ^2 fits provides a well defined strategy to disentangle the various influences and to estimate uncertainties in predictions. This is what we will unfold now in this section. Before carrying on, we want to remark that statistical analysis can unravel trends, uncertainties, and correlations for a given model. Be-

sides that we have to be aware of a systematic error which sneaks in by the choice of a functional form for the mean-field model. These can be explored by variation of a model and comparison of different models [92] as exemplified in [93]. We will not pursue the quest for systematic errors here.

4.2. Brief review of χ^2 analysis

The Skyrme-Hartree-Fock approximation is a typical representative of presently used self-consistent nuclear models. Its structure can be deduced from general arguments of low-momentum expansion [104, 105] while the remaining model parameters are determined by adjustment to empirical data, for reviews see [106, 107]. Strategies for such adjustment have much developed over the decades. Present standard are least-squares (χ^2) fits started in [108] and steadily extended to include more and more data, for recent examples see, *e.g.*, [100, 109]. The least-squares (χ^2) fits and subsequent analysis of extrapolation errors as well as correlations are a standard technique and well documented at several places [92, 110, 111]. The task is to optimise a set of model parameters $\mathbf{p} = (p_1, \dots, p_{N_p})$ such that a representative set of observables $\{\hat{O}_i, i = 1 \dots N_d\}$ is optimally reproduced. This is achieved by defining a quality function $\chi^2(\mathbf{p})$ from the sum of squared errors and minimising it. Extrapolation uncertainties and correlations between observables can be estimated from the behaviour of χ^2 in the vicinity of the minimum. To that end, one defines probability distribution of “reasonable” parametrisations as $W(\mathbf{p}) \propto \exp(-\frac{1}{2}\chi^2(\mathbf{p}))$. The (statistical) expectation value of an observable \hat{A} is then $\bar{A} = \int d^{N_p} p A(\mathbf{p}) W(\mathbf{p})$. Extrapolation uncertainties quantify the fluctuation around the mean value and are computed as $\Delta A = \sqrt{(A - \bar{A})^2}$. The correlation between A and B , also called covariance, becomes $c_{AB} = \overline{(A - \bar{A})(B - \bar{B})} / (\Delta A \Delta B)$. The actual evaluation is usually done in terms of Gaussian integrals because χ^2 can be well approximated by a quadratic form in \mathbf{p} , see *e.g.* [92].

4.3. Choice of fit observables and force parameters

For the fit observables entering the χ^2 , we consider here the same set as it was used in the survey [100]: binding energies, key parameters of the charge form factor (r.m.s. radius, diffraction radius, surface thickness), odd-even staggering of binding energies, spin-orbit splittings in semi-magic nuclei selected to be well described by a pure mean-field model. A straightforward fit to these ground state data yields the parametrisation SV-min. It embraces all information how the given ground state data determine features of the parametrisation and how much they leave undetermined.

A key feature of a model are the nuclear matter properties (NMP). We will consider here the four NMP which characterise the response properties of nuclear matter: incompressibility K , isoscalar effective mass m^*/m , symmetry energy a_{sym} , and TRK sum-rule enhancement κ_{TRK} (for a detailed definition see *e.g.*, [100]). These NMP have been used since long as benchmarks in various nuclear models and thus they have developed an intuitive meaning. Moreover, there is a one to one relation between NMP and the force parameters of the volume part of the SHF functional. Thus NMP are equivalent to force parameters. Dedicated variation of NMP is useful tool to explore influences within a model. Thus we will also consider parametrisations which are fitted as SV-min, but with an additional constraint on NMP. There is, for example, the parametrisation SV-bas which was fitted while freezing K , m^*/m , a_{sym} , and κ_{TRK} at values such that one

obtains additionally also a good description of giant resonance excitations [100]. The difference between SV-bas and SV-min is one indicator for the influence the these four NMP. We will consider in section 4.6 an even greater variation of parametrisations.

4.4. Extrapolation uncertainties

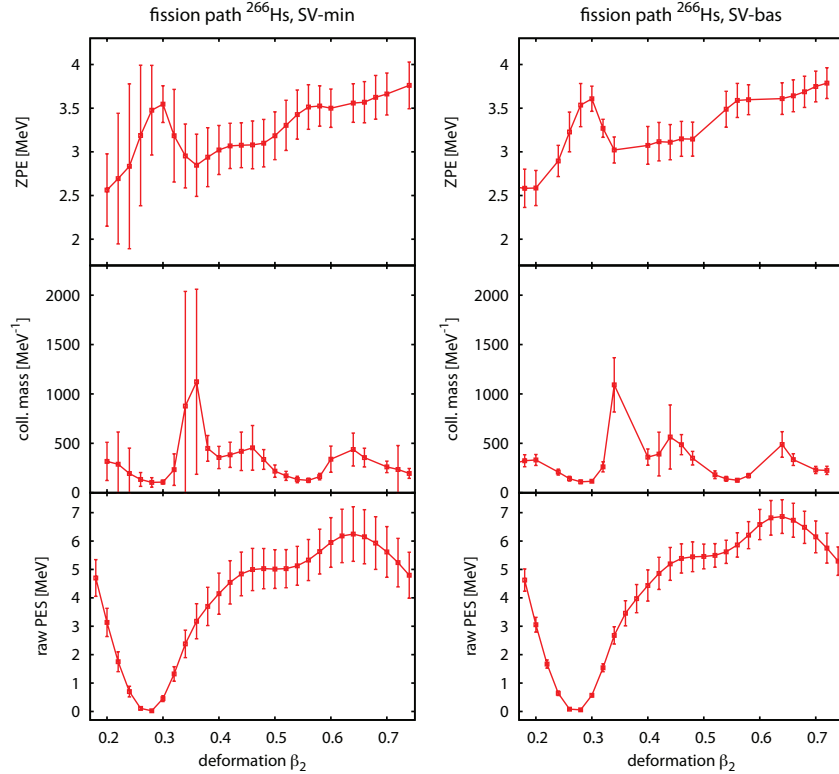


Figure 14: Raw PES (lower panels), mass parameter (middle panels), and ZPE (upper panels) along the axial and reflection symmetric fission path of ^{266}Hs . The left panels show results for SV-min, the right ones for SV-bas. Each case is shown together with the extrapolation uncertainties from χ^2 analysis.

Uncertainties for extrapolated observables are the simpler signal from χ^2 analysis. Thus we start with a quick glance at uncertainties for the present test case, fission of ^{266}Hs . Figure 14 shows the ingredients for a fission calculation, potential-energy surface (PES), zero-point energy (ZPE) and mass parameter, all for motion along axially symmetric quadrupole deformation expressed as the dimension-less $q \equiv \beta_2$ (for details of the collective picture behind see, *e.g.*, [78, 50]). The figure label indicates “raw PES”. This is the energy directly from a quadrupole constraint SHF calculation. The collective fission dynamics employs the PES corrected by ZPE [78, 50]. The pattern for the corrected PES are very similar to those for the raw PES and thus we have skipped this extra panel. The mass parameter is obtained by self-consistent cranking, also called ATDHF cranking [78, 50]. All three quantities are shown together with the extrapolation uncertainties from χ^2 analysis (see section 4.2) drawn as error bars. Note that the PES are scaled to zero energy at the minimum. There is thus no uncertainty at this point and only slowly growing

uncertainty around it. Sufficiently far away from the minimum, the error bars are of similar size along the path. The same holds for the ZPE. More fluctuations of uncertainties are seen for the the mass parameter. Some points have very large uncertainties and some points for SV-bas did not produce a reasonable result at all (that is why there are missing points in the curves). These artifacts are due to round-off problems in the very demanding error analysis combined with the demanding computation of mass parameters. These problems arise typically in regions where many level crossing exist.

The uncertainties for the unconstrained fit SV-min are larger than those for SV-bas. This is plausible because SV-bas is constrained by four NMP which reduces uncertainties. However, the reduction is only about factor two. The constraint on K , m^*/m , a_{sym} , κ_{TRK} thus has only partially impact on fission properties. There remains an equally strong influence from the other force parameters. The uncertainty of the PES at the barrier is 1 MeV for SV-min and 0.6 MeV for SV-bas. This shows the benefit of adding more information from NMP, alias giant resonances [100]. Still the uncertainty is large as compared to the extreme sensitivity of the fission lifetime. A prediction within four order of magnitudes is already great success [93].

4.5. Correlation analysis for the key observables

In a study of inter-correlations within the fission path (not shown here) we have found that the values of potential energy $V(\beta_2)$ along the fission path are highly correlated with each other which means, *e.g.*, that knowing the barrier height B_f determines the fission potential $V(\beta_2)$ in a broad vicinity around the barrier. The same hold for the mass parameter. This allows to reduce the relevant information to the few key observables as indicated in figure 12. We will henceforth reduce the discussion to these. Figure 15 shows the matrix of correlations between forces parameters and key observables of the fission path for SV-min. Remind that many of the SHF force parameters can be mapped to NMP which are a more intuitive way to characterise a force. The five bulk parameters of the SHF functional (volume term, density dependent term) can be represented by the five NMP equilibrium binding E/A with ρ_0 , incompressibility K , symmetry energy a_{sym} and slope thereof $\partial_\rho a_{\text{sym}}$. The two parameters for kinetic terms correspond to the two NMP for effective mass, m^*/m and κ_{TRK} . The two parameters for the gradient terms correspond to the two surface energies a_{surf} and $a_{\text{surf,sym}}$ computed here in semi-classical approximation [112]. Only pairing and spin-orbit parameters have no bulk equivalent and remain what they are.

Amongst the key observables of the path (see figure 12), we see a strong correlation between barrier B_f and curvature $\partial^2 E(q)/\partial q^2|_{q_{\text{min}}}$, some correlation between these two quantities and the action integral, and very little correlation to the mass parameter at ground state. What the correlations of fission properties with force parameters is concerned, they are mostly small. Only m^*/m and pairing parameters show some correlations, pairing particularly with the mass parameter and m^*/m with the barrier. After all, we see that there is no pronounced correlation of a fission observables to any particular force parameter. This indicates that each detail of the force contributes a bit to fission where from pairing is the strongest player.

4.6. Trend analysis for the key observables of ^{266}Hs

Covariance analysis is a powerful tool to find out dependencies between observables (and force parameters). But it often lacks intuitive insight. As a complementing tool, one can perform a trend analysis. This is done by producing systematically various sets of forces where in each set one forces parameter (or NMP) is varied. Such sets had been produced in [100] starting with SV-bas as base point. The sets were obtained by constraining the same four NMP as for SV-bas

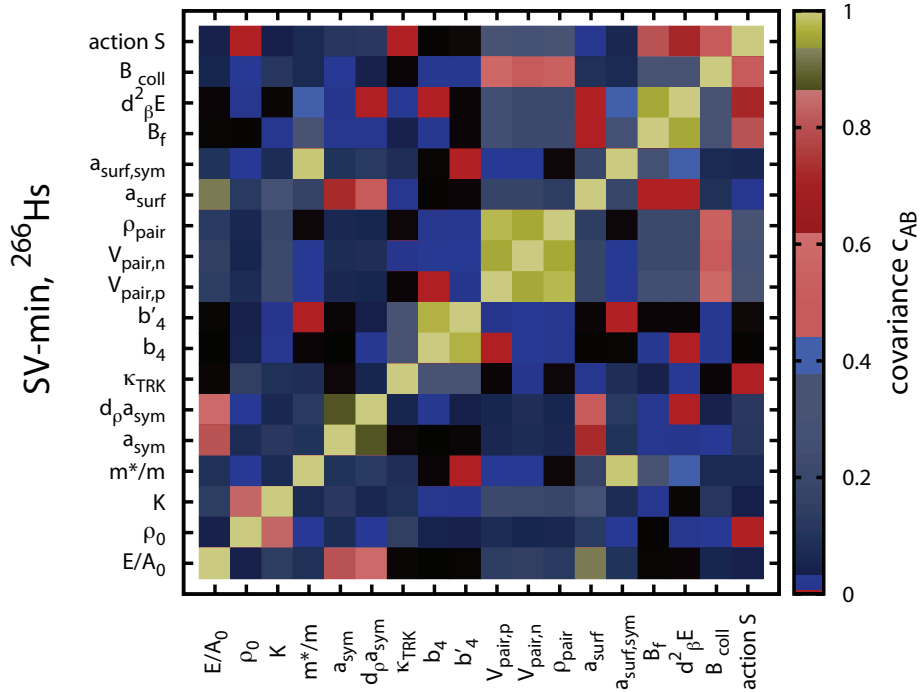


Figure 15: Matrix of correlations between the key observables of the fission path in ^{266}Hs for selected force parameters SV-min.

while varying one of the four NMP with respect to SV-bas. One can then draw the observables of interest versus the varied parameter. This makes the dependencies graphically visible which is often a helpful complementing illustration of the correlation.

Figure 16 illustrates the influences on fission in terms of the trends with the force parameters (NMP, respectively) K , m^*/m , a_{sym} , κ_{TRK} , and pairing strength. In order to compare the trends within one panel (for each observable), we produced dimensionless force parameters. This is done by taking the parameters relative to the SV-bas point and scaled by the uncertainty from SV-min which characterises the allowed variation, *i.e.* the rescaled version of a parameter p is $p_{\text{rescal}} = (p - p_{\text{SV-bas}})/\Delta p_{\text{SV-min}}$. This implies that the interval of rescaled force parameters $[-1, +1]$ represents the range of reasonable parameters for which the reproduction of data remains nearly as good as for the minimum (χ^2 growing at most by one unit [110, 111, 92]).

The trends in Figure 16 confirm what we have seen already from the correlation matrix. Pairing strength has the strongest impact on fission. Next important is m^*/m . There is also some impact from a_{sym} , but K as well as κ_{TRK} play little role here in SHF.

5. Summary and outlook

We have presented a variety of theoretical results on fission properties in super-heavy nuclei. Rather different modelling has been compared, the macroscopic-microscopic (MM) method, on the one hand, and self-consistent mean-field models on the other. The basis of the description

	K [MeV]	m^*/m	a_{sym} [MeV]	κ_{TRK}	V_{prot} [MeV fm $^{-3}$]	V_{neut} [MeV fm $^{-3}$]
param.	233.5	0.9	30	0.4	675	607
Δ param.	8.5	0.07	1.9	0.3	25	39

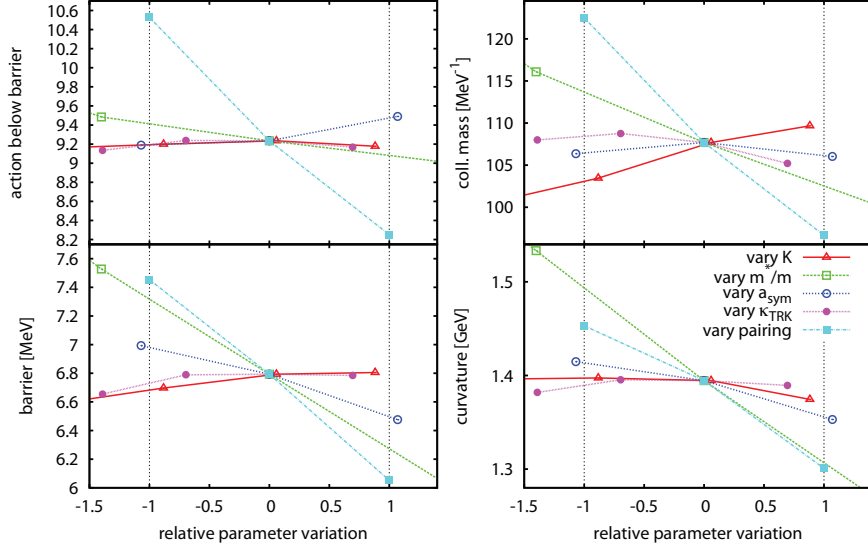


Figure 16: Trends of the key observables of the fission path of ^{266}Hs with systematically varied force parameters. The parameters are drawn relative to their reference value from SV-bas and scaled to the extrapolation uncertainty of SV-min. These reference values and their uncertainties are given in the table above the plots. The values ± 1 for the scaled parameters stands for the variance shown in the table. The band ± 1 for the scaled parameters represents the allowed error band from χ^2 analysis.

is the same in both model families: the state of the system is characterised by a set of single-particle (SP) wavefunctions moving in a common mean-field and the fission path consists in a series of such states with successively increasing deformation until two separated fragments emerge. The SP wavefunctions serve to account properly for the quantum shell effects which are crucial for binding of heavy elements and the topology of the potential energy surface. The fact that a couple of different mean-field states is involved means that the description deals, in fact, with collectively correlated states. These features are the same for all models. Different is the way in which the mean field and the total energy are defined. The MM method models the mean-field directly as a (deformed) shell-model potential and composes the total energy from the macroscopic liquid-drop model plus shell corrections deduced from the s.p. energies. Self-consistent models start from an energy-density functional where-from the mean-field equations are derived variationally. The dedicated deformation which are needed to span the fission path are obtained by adding a (quadrupole) constraint. The density functionals manage to incorporate a correct description of bulk properties (liquid-drop parameters) together with shell structure. Within the self-consistent family, we have considered three different models, the Skyrme-Hartree-Fock (SHF) approach which is a non-relativistic density-functional method, the Gogny force which, again, uses non-relativistic kinematics but a finite-range force with a sprinkle of density dependence, and the relativistic mean-field model (RMF) which relies on a covariant

Lagrangian density functional.

In spite of the very different modelling, the topological properties of the fission path are coming out the same way in all models: ground state deformations, fission isomers, shapes at barrier (reflection symmetry, triaxiality), islands of stability. These features are determined by quantum shell structure which is obviously correctly reproduced in all cases. Huge differences in the predictions are found in the quantitative aspects, height of fission barriers, and even more so for fission lifetimes. These values are very hard to control. Each detail of a model has an influence. Each one of the liquid-drop bulk properties has some impact on barriers, the effective mass which regulates shell effects plays also a role, and last not least pairing is a crucial ingredient. Statistical analysis on top of least-squares fits within the SHF approach estimates the uncertainties on barriers typically of the order of ± 1 MeV. We have to add substantial leeway for systematic errors which, however, cannot be estimated in systematic manner. The situation is even more involved for fission lifetimes. Further ingredients are required for its computation: entry point for spontaneous fission, collective mass along the path, and quantum corrections for spurious zero-point energies. All these are extremely subtle quantities which depend very sensitively on all details of a model and on the way they are computed. There is lot of development work yet to be done to reach better agreement in the quantitative predictions. For the time being, the method of choice is to calibrate barriers and lifetimes for the heaviest known nuclei to allow safer predictions for the even heavier elements.

Most self-consistent calculations describe fission as a one-dimensional, adiabatic process. MM calculations indicate that this may not always be sufficient. There are situations in which deformation valley and fission valley go in parallel for while. It is likely that one needs here a description in terms of multi-dimensional collective motion. This is an extremely challenging problem which has not been attacked thoroughly yet. We hope that increasing computing power allows steps into that direction. The quality of the adiabatic approximation deserves also critical testing. There exist already investigations on dynamical aspects of fission. This line of development needs also further inspection to learn more about the limits of presently used methods and possibly to improve on them.

Self-consistent models are optimized by least-squares fits to data. Trend- and correlations-analysis built on the underlying least-squares fits shows that the relations of fission properties and forces parameters and NMP are mixed. We see the reduction of uncertainties when fixing a couple of NMP. But there is no single NMP which has predominant influence. Fission properties depend on every detail of the parametrisation, the bulk properties given by NMP as well as pairing strength and spin-orbit coupling (determining shell effects).

All this shows that a proper description of fission is extremely demanding. More research is needed to achieve a higher reliability for predictions of fission lifetimes in the context of self-consistent mean-field models.

Acknowledgements. This work was supported by the Bundesministerium für Bildung und Forschung (BMBF) under contract number 05P12RFFTB; by Narodowe Centrum Nauki under grant no. 2011/01/B/ST2/05131. M.K. was co-financed by LEA COPIGAL funds, and the work of LMR was supported in part by Spanish MINECO grants Nos. FPA2012-34694 and FIS2012-34479 and by the Consolider-Ingenio 2010 program MULTIDARK CSD2009-00064.

References

- [1] Y. Oganessian, V. Utyonkov, Y. Lobanov, F. Abdullin, A. Polyakov, I. Shirokovsky, Y. Tsyganov, G. Gulbekian, S. Bogomolov, B. Gikal, A. Mezentsev, S. Iliev, V. Subbotin, A. Sukhov, G. Buklanov, K. Subotic, M. Itkis,

- K. Moody, J. Wild, N. Stoyer, M. Stoyer, R. Lougheed, *Phys. Rev. Lett.* 83 (1999) 3154–3157.
- [2] Y. T. Oganessian, A. V. Yeremin, A. G. Popeko, S. L. Bogomolov, G. V. Buklanov, M. L. Chelnokov, V. I. Chepigin, B. N. Gikal, V. A. Gorshkov, G. G. Gulbekian, M. G. Itkis, A. P. Kabachenko, A. Y. Lavrentev, O. N. Malyshev, J. Rohac, R. N. Sagaidak, S. Hofmann, S. Saro, G. Giardina, K. Morita, *Nature* 400 (1999) 242.
- [3] Y. Oganessian, V. Utyonkov, Y. Lobanov, F. Abdullin, A. Polyakov, I. Shirokovsky, Y. Tsyganov, G. Gulbekian, S. Bogomolov, B. Gikal, A. Mezentsev, S. Iliev, V. Subbotin, A. Sukhov, O. Ivanov, G. Buklanov, K. Subotic, M. Itkis, K. Moody, J. Wild, N. Stoyer, M. Stoyer, R. Lougheed, *Phys. Rev. C* 62 (2000) 041604.
- [4] Y. Oganessian, V. Utyonkov, Y. Lobanov, F. Abdullin, A. Polyakov, I. Shirokovsky, Y. Tsyganov, G. Gulbekian, S. Bogomolov, B. Gikal, A. Mezentsev, S. Iliev, V. Subbotin, A. Sukhov, O. Ivanov, G. Buklanov, K. Subotic, M. Itkis, K. Moody, J. Wild, N. Stoyer, M. Stoyer, R. Lougheed, C. Laue, Y. Karelin, A. Tatarinov, *Phys. Rev. C* 63 (2000) 011301.
- [5] Y. Oganessian, V. Utyonkov, Y. Lobanov, F. Abdullin, A. Polyakov, I. Shirokovsky, Y. Tsyganov, G. Gulbekian, S. Bogomolov, B. Gikal, A. Mezentsev, S. Iliev, V. Subbotin, A. Sukhov, A. Voinov, G. Buklanov, K. Subotic, V. Zagrebaev, M. Itkis, J. Patin, K. Moody, J. Wild, M. Stoyer, N. Stoyer, D. Shaughnessy, J. Kenneally, R. Lougheed, *Phys. Rev. C* 69 (2004) 054607.
- [6] Y. Oganessian, F. Abdullin, P. Bailey, D. Benker, M. Bennett, S. Dmitriev, J. Ezold, J. Hamilton, R. Henderson, M. Itkis, Y. Lobanov, A. Mezentsev, K. Moody, S. Nelson, A. Polyakov, C. Porter, A. Ramayya, F. Riley, J. Roberto, M. Ryabinin, K. Rykaczewski, R. Sagaidak, D. Shaughnessy, I. Shirokovsky, M. Stoyer, V. Subbotin, R. Sudowe, A. Sukhov, Y. Tsyganov, V. Utyonkov, A. Voinov, G. Vostokin, P. Wilk, *Phys. Rev. Lett.* 104 (2010) 142502.
- [7] Y. Oganessian, V. Utyonkov, Y. Lobanov, F. Abdullin, A. Polyakov, R. Sagaidak, I. Shirokovsky, Y. Tsyganov, A. Voinov, G. Gulbekian, S. Bogomolov, B. Gikal, A. Mezentsev, S. Iliev, V. Subbotin, A. Sukhov, K. Subotic, V. Zagrebaev, G. Vostokin, M. Itkis, K. Moody, J. Patin, D. Shaughnessy, M. Stoyer, N. Stoyer, P. Wilk, J. Kenneally, J. Landrum, J. Wild, R. Lougheed, *Phys. Rev. C* 74 (2006) 044602.
- [8] Y. Oganessian, V. Utyonkov, Y. Lobanov, F. Abdullin, A. Polyakov, R. Sagaidak, I. Shirokovsky, Y. Tsyganov, A. Voinov, A. Mezentsev, V. Subbotin, A. Sukhov, K. Subotic, V. Zagrebaev, S. Dmitriev, R. Henderson, K. Moody, J. Kenneally, J. Landrum, D. Shaughnessy, M. Stoyer, N. Stoyer, P. Wilk, *Phys. Rev. C* 79 (2009) 024603.
- [9] Y. Oganessian, F. Abdullin, C. Alexander, J. Binder, R. Boll, S. Dmitriev, J. Ezold, K. Felker, J. Gostic, R. Grzywacz, J. Hamilton, R. Henderson, M. Itkis, K. Miernik, D. Miller, K. Moody, A. Polyakov, A. Ramayya, J. Roberto, M. Ryabinin, K. Rykaczewski, R. Sagaidak, D. Shaughnessy, I. Shirokovsky, M. Shumeiko, M. Stoyer, N. Stoyer, V. Subbotin, A. Sukhov, Y. Tsyganov, V. Utyonkov, A. Voinov, G. Vostokin, *Phys. Rev. Lett.* 109 (2012) 162501.
- [10] S. Liu, J. Hamilton, A. Ramayya, S. Zhu, Y. Shi, F. Xu, J. Batchelder, N. Brewer, J. Hwang, Y. Luo, J. Rasmussen, W. Ma, A. Daniel, G. Ter-Akopian, Y. Oganessian, *Phys. Rev. C* 87 (2013) 057302.
- [11] Y. T. Oganessian, F. S. Abdullin, C. Alexander, J. Binder, R. Boll, S. Dmitriev, J. Ezold, K. Felker, J. Gostic, R. Grzywacz, J. Hamilton, R. Henderson, M. Itkis, K. Miernik, D. Miller, K. Moody, A. Polyakov, A. Ramayya, J. Roberto, M. Ryabinin, K. Rykaczewski, R. Sagaidak, D. Shaughnessy, I. Shirokovsky, M. Shumeiko, M. Stoyer, N. Stoyer, V. Subbotin, A. Sukhov, Y. S. Tsyganov, V. Utyonkov, A. Voinov, G. Vostokin, *Phys. Rev. C* 87 (2013) 054621.
- [12] F. Heßberger, S. Hofmann, V. Ninov, P. Armbruster, H. Folger, G. Münzenberg, H. Schtt, A. Popeko, A. Yeremin, A. Andreyev, S. Saro, *Zeitschrift für Physik A Hadrons and Nuclei* 359 (1997) 415–425.
- [13] G. Münzenberg, P. Armbruster, H. Folger, P. Heßberger, S. Hofmann, J. Keller, K. Poppensieker, W. Reisdorf, K.-H. Schmidt, H.-J. Schtt, M. Leino, R. Hingmann, *Z. Phys. A Atoms and Nuclei* 317 (2) (1984) 235–236.
- [14] S. Hofmann, *Rep. Prog. Phys.* 61 (1998) 639.
- [15] Hofmann, S., Heinz, S., Mann, R., Maurer, J., Khuyagbaatar, J., Ackermann, D., Antalic, S., Barth, W., Block, M., Burkhard, H. G., Comas, V. F., Dahl, L., Eberhardt, K., Gostic, J., Henderson, R. A., Heredia, J. A., Heßberger, F. P., Kenneally, J. M., Kindler, B., Kojouharov, I., Kratz, J. V., Lang, R., Leino, M., Lommel, B., Moody, K. J., Münzenberg, G., Nelson, S. L., Nishio, K., Popeko, A. G., Runke, J., Saro, S., Shaughnessy, D. A., Stoyer, M. A., Thrlle-Pospiech, P., Tinschert, K., Trautmann, N., Uusitalo, J., Wilk, P. A., Yeremin, A. V., *Eur. Phys. J. A* 48 (2012) 62.
- [16] C. Düllmann, M. Schädel, A. Yakushev, A. Türler, K. Eberhardt, J. Kratz, D. Ackermann, L.-L. Andersson, M. Block, W. Bröchle, J. Dvorak, H. Essel, P. Ellison, J. Even, J. Gates, A. Gorshkov, R. Graeger, K. Gregorich, W. Hartmann, R.-D. Herzberg, F. Heßberger, D. Hild, A. Hübner, E. Jäger, J. Khuyagbaatar, B. Kindler, J. Krier, N. Kurz, S. Lahiri, D. Liebe, B. Lommel, M. Maiti, H. Nitsche, J. Omtvedt, E. Parr, D. Rudolph, J. Runke, B. Schausten, E. Schimpf, A. Semchenkov, J. Steiner, P. Thörle-Pospiech, J. Uusitalo, M. Wegrzecki, N. Wiehl, *Phys. Rev. Lett.* 104 (2010) 252701.
- [17] L. Stavsetra, K. Gregorich, J. Dvorak, P. Ellison, I. Dragojević, M. Garcia, H. Nitsche, *Phys. Rev. Lett.* 103 (2009) 132502.

- [18] H. Haba, D. Kaji, H. Kikunaga, Y. Kudou, K. Morimoto, K. Morita, K. Ozeki, T. Sumita, A. Yoneda, Y. Kasamatsu, Y. Komori, K. Ooe, A. Shinohara, *Phys. Rev. C* 83 (2011) 034602.
- [19] P. Reiter, T. Khoo, C. Lister, D. Seweryniak, I. Ahmad, M. Alcorta, M. Carpenter, J. Cizewski, C. Davids, G. Gervais, J. Greene, W. Henning, R. Janssens, T. Lauritsen, S. Siem, A. Sonzogni, D. Sullivan, J. Uusitalo, I. Wiedenhöver, N. Amzal, P. Butler, A. Chewter, K. Ding, N. Fotiades, J. Fox, P. Greenlees, R.-D. Herzberg, G. Jones, W. Kortzen, M. Leino, K. Vetter, *Phys. Rev. Lett.* 82 (1999) 509–512.
- [20] S. Ćwiok, J. Dobaczewski, P.-H. Heenen, P. Magierski, W. Nazarewicz, *Nucl. Phys. A* 611 (1996) 211–246.
- [21] S. Ćwiok, P.-H. Heenen, W. Nazarewicz, *Nature* 433 (2005) 705.
- [22] A. Sobiczewski, K. Pomorski, *Prog. Part. Nucl. Phys.* 58 (2007) 292–349.
- [23] M. Warda, L. M. Robledo, *Phys. Rev. C* 84 (2011) 044608.
- [24] M. Warda, J. L. Egido, *Phys. Rev. C* 86 (2012) 014322.
- [25] A. Staszczak, A. Baran, W. Nazarewicz, *Phys. Rev. C* 87 (2013) 024320.
- [26] J. A. Sheikh, W. Nazarewicz, J. C. Pei, *Phys. Rev. C* 80 (2009) 011302.
- [27] J. C. Pei, W. Nazarewicz, J. A. Sheikh, A. K. Kerman, *Phys. Rev. Lett.* 102 (2009) 192501.
- [28] A. Baran, J. A. Sheikh, J. Dobaczewski, W. Nazarewicz, A. Staszczak, *Phys. Rev. C* 84 (2011) 054321.
- [29] J. Sadhukhan, K. Mazurek, A. Baran, J. Dobaczewski, W. Nazarewicz, J. A. Sheikh, *Phys. Rev. C* 88 (2013) 064314.
- [30] J. Sadhukhan, J. Dobaczewski, W. Nazarewicz, J. A. Sheikh, A. Baran, *Phys. Rev. C* 90 (2014) 061304(R).
- [31] N. Schindzielorz, J. Erler, P. Klüpfel, P.-G. Reinhard, G. Hager, *Int. J. Mod. Phys. E* 18 (2009) 773.
- [32] M. Kowal, P. Jachimowicz, A. Sobiczewski, *Phys. Rev. C* 82 (2010) 014303.
- [33] M. Kowal, A. Sobiczewski, *Int. J. Mod. Phys. E* 18 (04) (2009) 914–918.
- [34] A. Sobiczewski, M. Kowal, *Physica Scripta* 2006 (T125) (2006) 68.
- [35] P. Möller, A. J. Sierk, T. Ichikawa, A. Iwamoto, R. Bengtsson, H. Uhrenholt, S. Aberg, *Phys. Rev. C* 79 (2009) 064304.
- [36] H. Abusara, A. V. Afanasjev, P. Ring, *Phys. Rev. C* 85 (2012) 024314.
- [37] S. Ćwiok, J. Dudek, W. Nazarewicz, J. Skalski, T. Werner, *Comput. Phys. Commun.* 46 (1987) 379.
- [38] V. Strutinsky, *Nucl. Phys. A* 95 (1967) 420.
- [39] V. Strutinsky, *Nucl. Phys. A* 122 (1968) 1.
- [40] J. R. Krappe, H.J. Nix, A. J. Sierk, *Phys. Rev. C* 20 (1979) 992.
- [41] Z. Muntian, I. Patyk, A. Sobiczewski, *Acta Phys. Pol. B* 32 (2001) 691.
- [42] G. Audi, O. Bersillon, J. Blachot, A. H. Wapstra, *Nucl. Phys. A* 624.
- [43] A. Staszczak, J. Dobaczewski, W. Nazarewicz, *Int. J. Mod. Phys. E* 14 (2005) 395.
- [44] A. Staszczak, J. Dobaczewski, W. Nazarewicz, *Int. J. Mod. Phys. E* 16 (2007) 310.
- [45] P. Jachimowicz, M. Kowal, J. Skalski, *Phys. Rev. C* 85 (2012) 034305.
- [46] P. Möller, A. J. Sierk, T. Ichikawa, A. Iwamoto, M. Mumpower, *phys. Rev. C* - accepted, report LA-UR-14-249 (2006).
- [47] D. Vautherin, D. M. Brink, *Phys. Rev. C* 5 (1972) 626.
- [48] D. Vautherin, *Phys. Rev. C* 7 (1973) 298–316.
- [49] J. Bartel, P. Quentin, M. Brack, C. Guet, H. Håkansson, *Nuclear Physics A* 386 (1982) 79.
- [50] J. Erler, K. Langanke, H. P. Loens, G. Martinez-Pinedo, P.-G. Reinhard, *Phys. Rev. C* 85 (2012) 025802.
- [51] M. Warda, J. Egido, L. M. Robledo, P. K., *Phys. Rev. C* 66 (2002) 014310.
- [52] J. Libert, M. Girod, J.-P. Delaroche, *Phys. Rev. C* 60 (1999) 054301.
- [53] Y. T. Oganessian, *Acta Phys. Pol. B* 43 (2012) 167.
- [54] L. I. Schiff, *Quantum mechanics*, McGraw-Hill, 1949.
- [55] D. Geldart, D. Kiang, *Am. J. Phys.* 54.
- [56] A. Baran, Z. Łojewski, K. Sieja, M. Kowal, *Phys. Rev. C* 72 (2005) 044310–1–13.
- [57] P.-H. Heenen, J. Skalski, A. Staszczak, A. Vretenar, *Shapes, deformations, α and β -decays*, *Nucl. Phys.*, this volume.
- [58] A. Baran, A. Staszczak, *Acta Phys. Pol.* 45 (2014) 273.
- [59] V. E. Jr. Viola, G. T. Seaborg, *J. Inorg. Nucl. Chem.* 28 (1966) 741.
- [60] A. Parkhomenko, A. Sobiczewski, *Acta Phys. Pol. B* 36 (2005) 3095.
- [61] M. M. Kortelainen, J. McDonnell, W. Nazarewicz, P.-G. Reinhard, J. Sarich, N. Schunck, M. V. Stoitsov, S. M. Wild, *Phys. Rev. C* 85 (2012) 024304.
- [62] D. Gogny, *Nuclear Self-consistent fields*, North-Holland, Amsterdam, 1975.
- [63] T. H. R. Skyrme, *Phil. Mag.* 1 (1956) 1043–1054.
- [64] V. Martin, L. M. Robledo, *Int. J. Mod. Phys. E* 18 (04) (2009) 861–868.
- [65] S. Perez-Martin, L. M. Robledo, *Int. J. of Mod. Phys. E* 18 (2009) 788–797.
- [66] G. Henning, T. L. Khoo, A. Lopez-Martens, D. Seweryniak, M. Alcorta, M. Asai, B. B. Back, P. F. Bertone, D. Boilley, M. P. Carpenter, C. J. Chiara, P. Chowdhury, B. Gall, P. T. Greenlees, G. Gürdal, K. Hauschild,

- A. Heinz, C. R. Hoffman, R. V. F. Janssens, A. V. Karpov, B. P. Kay, F. G. Kondev, S. Lakshmi, T. Lauritsen, C. J. Lister, E. A. McCutchan, C. Nair, J. Piot, D. Potterveld, P. Reiter, A. M. Rogers, N. Rowley, S. Zhu, *Phys. Rev. Lett.* 113 (2014) 262505.
- [67] J. L. Egido, L. M. Robledo, *Phys. Rev. Lett.* 85 (2000) 1198–1201.
- [68] R. Rodríguez-Guzmán, L. M. Robledo, *Phys. Rev. C* 89 (2014) 054310.
- [69] R. Rodríguez-Guzmán, L. Robledo, *Eur. Phys. J. A* 50 (9).
- [70] S. A. Giuliani, L. M. Robledo, R. Rodríguez-Guzmán, *Phys. Rev. C* 90 (2014) 054311.
- [71] J. Dechargé, J.-F. Berger, K. Dietrich, M. Weiss, *Physics Letters B* 451 (3–4) (1999) 275 – 282.
- [72] J.-F. Berger, L. Bitaud, J. Dechargé, M. Girod, K. Dietrich, *Nuclear Physics A* 685 (1–4) (2001) 1 – 16, nucleus-Nucleus Collisions 2000.
- [73] J. Berger, D. Hirata, M. Girod, *Acta Phys. Pol. B* 34 (2003) 1909.
- [74] J. Dechargé, J.-F. Berger, M. Girod, K. Dietrich, *Nuclear Physics A* 716 (0) (2003) 55 – 86.
- [75] J. F. Berger, D. Hirata, M. Girod, J. Decharge, *Int. J. Mod. Phys. E* 13 (01) (2004) 79–86.
- [76] M. Warda, J. L. Egido, L. M. Robledo, *Int. J. Mod. Phys. E* 15 (2006) 504–510.
- [77] M. Warda, *Int. J. Mod. Phys. E* 16 (2007) 452–458.
- [78] P.-G. Reinhard, K. Goeke, *Rep. Prog. Phys.* 50 (1987) 1.
- [79] M. J. Giannoni, P. Quentin, *Phys. Rev. C* 21 (1980) 2060–2075.
- [80] M. J. Giannoni, P. Quentin, *Phys. Rev. C* 21 (1980) 2076–2093.
- [81] R. Smolańczuk, J. Skalski, A. Sobiczewski, *Phys. Rev. C* 52 (1995) 1871.
- [82] T. Bürvenich, M. Bender, J. A. Maruhn, P.-G. Reinhard, *Phys. Rev. C* 69 (2004) 014307.
- [83] E. E. Chabanat, P. Bonche, P. Haensel, J. Meyer, R. Schaefer, *Nucl. Phys. A* 635 (1998) 231.
- [84] A. Mamdouh, J. M. Pearson, M. Rayet, F. Tondeur, *Nucl. Phys. A* 679 (2001) 337.
- [85] M. G. Itkis, Y. T. Oganessian, V. I. Zagrebaev, *Phys. Rev. C* 65 (2002) 044602.
- [86] K. Siwek-Wilczyńska, A. Borowiec, J. Wilczyński, *Int. J. Mod. Phys. E* 18 (2009) 1079.
- [87] K. Siwek-Wilczyńska, T. Cap, J. Wilczyński, *Int. J. Mod. Phys. E* 19 (2010) 500.
- [88] A. Baran, *Phys. Lett.* 76B (1978) 8–10.
- [89] A. Baran, K. Pomorski, A. Łukasiak, S. A., *Nucl. Phys. A* 361 (1981) 83.
- [90] J. Sadhukhan, K. Mazurek, J. Dobaczewski, W. Nazarewicz, J. A. Sheikh, A. Baran, *Acta Phys. Pol. B* (2014) accepted for publication.
- [91] S. Piłat, A. Staszczak, K. Pomorski, 50 years with nuclear fission, in: A. D. Carlson, J. W. Behrens (Eds.), *50 Years with Nuclear Fission*, National Academy of Science, National Institute of Standards and Technology, American Nuclear Society, Inc., 1989, pp. 637–642.
- [92] J. Dobaczewski, W. Nazarewicz, P.-G. Reinhard, *J. Phys. G* 41 (2014) 074001.
- [93] J. Erler, P.-G. Reinhard, *J. Phys.* to appear.
- [94] J. Dechargé, D. Gogny, *Phys. Rev. C* 21 (1980) 1568–1593.
- [95] J. Dobaczewski, H. Flocard, J. Treiner, *Nucl. Phys. A* 422 (1984) 103–139.
- [96] F. Tondeur, M. Brack, M. Farine, J. Pearson, *Nucl. Phys. A* 420 (1984) 297.
- [97] E. Chabanat, P. Bonche, P. Haensel, J. Meyer, R. Schaeffer, *Nucl. Phys. A* 627 (1997) 710–746.
- [98] P.-G. Reinhard, H. Flocard, *Nucl. Phys. A* 584 (1995) 467–488.
- [99] M. Samyn, S. Goriely, P.-H. Heenen, J. M. Pearson, F. Tondeur, *Nucl. Phys. A* 700 (2002) 142–156.
- [100] P. Klüpfel, P.-G. Reinhard, T. J. Bürvenich, J. A. Maruhn, *Phys. Rev. C* 2009 (79) 034310.
- [101] M. Kortelainen, J. McDonnell, W. Nazarewicz, E. Olsen, P.-G. Reinhard, J. Sarich, N. Schunck, S. M. Wild, D. Davesne, J. Erler, A. Pastore, *Phys. Rev. C* 89 (2014) 054314.
- [102] M. Bender, K. Rutz, P.-G. Reinhard, J. A. Maruhn, W. Greiner, *Phys. Rev. C* 60 (1999) 034304.
- [103] W. Nazarewicz, P.-G. Reinhard, W. Satuła, D. Vretenar, *Eur. Phys. J. A* 50 (2014) 20.
- [104] J. W. Negele, D. Vautherin, *Phys. Rev. C* 5 (1972) 1472.
- [105] P.-G. Reinhard, C. Toepffer, *Int. J. Mod. Phys. E* 3 (1994) 435.
- [106] M. Bender, P.-H. Heenen, P.-G. Reinhard, *Rev. Mod. Phys.* 75 (2003) 121.
- [107] J. Stone, P.-G. Reinhard, *Prog. Part. Nucl. Phys.* 58 (2007) 587.
- [108] J. Friedrich, P.-G. Reinhard, *Phys. Rev. C* 33 (1986) 335.
- [109] M. Kortelainen, T. Lesinski, J. Moré, W. Nazarewicz, J. Sarich, N. Schunck, M. V. Stoitsov, S. Wild, *Phys. Rev. C* 82 (2010) 024313.
- [110] S. Brandt, *Statistical and computational methods in data analysis*, Springer, New York, 1997.
- [111] P. R. Bevington, D. K. Robinson, *Data Reduction and Error Analysis for the Physical Sciences*, McGraw-Hill, 2003.
- [112] W. Stocker, *Phys. Lett. B* 104 (1981) 339.